IBM Document Number TR-45-33

SPECIAL ROD SYSTEM STUDIES

SIXTH QUARTERLY REPORT

IBM

IBM Document Number TR-45-33

Special AROD System Studies

15 April 1965

Sixth Quarterly Report for NASA Contract No. NAS 8-11050

PREPARED FOR

GEORGE C. MARSHALL SPACE FLIGHT CENTER
NASA
HUNTSVILLE, ALABAMA

INTERNATIONAL BUSINESS MACHINES CORPORATION
Federal Systems Division
ROCKVILLE, MARYLAND

ABSTRACT

This document is the Sixth Quarterly Report on NASA Contract No. NAS 8-11050, Special AROD System Studies. It reviews the major conclusions on the Wideband Modulation Techniques task since its inception in October, 1964, and summarizes the work performed on the Wideband Modulation Techniques task and the Phase-Lock Loop task during the quarter ending March 31, 1965.

Section 1 (Review of Modulation Recommendations) presents the rationale for reaching the three major conclusions and recommendations concerning the wideband modulation techniques. These conclusions are:

a. Linear amplification should be employed in the spacecraft receiver.

b. A "hybrid" modulation waveform (combining a periodic signal with a pseudo-noise sequence) is preferable to a pure pseudo-noise waveform.

c. Common channel operation is not recommended because it would result in a very limited dynamic range.

Section 2 (Phase-Lock Loop Advanced Circuit Investigations) details the design characteristics of an analog memory implementation, using advanced semiconductor devices, to be incorporated in the Type I loop engineering model for purposes of achieving rapid reacquisition after short signal drop-outs.

Section 3 (Spectrum and Reacquisition Analysis) presents several methods for obtaining the rf spectrum from the angle modulation of a carrier with a filtered pseudo-noise signal, and presents the results of the investigation of reacquisition techniques for pseudo-noise signals.

CONTENTS

		Page
Section 1	REVIEW OF MODULATION RECOMMENDATIONS	1-1
1.1	Introduction	1-2
1.2	Linear Processing	1-2
1.3	Hybrid System	1-9
1.4	Common Channel Evaluation	1-13
Section 2	PHASE-LOCK LOOP ADVANCED CIRCUIT INVESTIGATION	2-1
2.1	Design Approach for Memory Aided Phase-Lock Loop	2-1
2.2	Design Considerations	2-2
2.3	Memory-Aiding Implementation	2-6
Section 3	SPECTRUM AND REACQUISITION ANALYSIS	3-1
3.1	Spectrum Analysis	3-1
3.2	Reacquisition Analysis	3-11
Appendix A	SEMICONDUCTOR DEVICES	A-1

ILLUSTRATIONS

Figure		Page
1-1	Amplitude Ratio and Suppression Factor Ratio Versus Range	1-6
1-2	Phase Error Versus Range	1-7
1-3	Comparison of Power Requirements for Pure PN System (P_s) and Hybrid System (S)	1-12
1-4	Envelope of Received PN Power Spectral Density	1-15
2-1	Block Diagram of Memory-Aided Phase-Locked Loop	2-4
2-2	Loop Filter and Amplifier	2-7
2-3	Loop Filter and Amplifier Equivalent Circuit	2-9
2-4	Loop Memory, Basic Circuit Configuration	2-10
2-5	Loop Memory, Schematic	2-12
2-6	Mode Detector and Loop Controls	2-13
3-1	Autocorrelation Function and Power Spectral Density of Psuedo-Noise Sequence	3-4

TABLES

Table		Page
2-1	Parameters of Memory-Aided Phase-Lock Loop (Carrier Tracking Filter Case)	2-3
3-1	Reacquisition Time Calculations for h = 400 Nautical Miles	3-15

Section 1

REVIEW OF MODULATION RECOMMENDATIONS

1.1 INTRODUCTION AND SUMMARY

This section reviews the major conclusions on the Wideband Modulation Techniques task since its inception in October, 1964. The purposes of the task are to analyze and evaluate wideband modulation techniques for use in the AROD system and to recommend the technique(s) most suitable for implementation.

In the previous Quarterly Report* many conclusions, recommendations, and derivations concerning the Wideband Modulation Techniques task were presented. It is the intention of this section to review the most important of the conclusions and the most significant steps and equations in their justification. Frequent references will be made to the Fifth Quarterly Report to avoid the necessity for lengthy derivations.

The three major conclusions concerning the wideband modulation techniques are:

1. Linear amplification should be employed in the spacecraft receiver.
2. A "hybrid" modulation waveform (combining a periodic signal with a pseudo-noise sequence) is preferable to a pure pseudo-noise waveform.
3. Common channel operation is not recommended because it would result in a very limited dynamic range.

The rationale behind the first conclusion is presented in Sub-section 1.2. The adaptivity inherent in the linear implementation is shown to be extremely advantageous in meeting the overall AROD system requirements; limiting or

---

* Special AROD System Studies, Fifth Quarterly Report, International Business Machines Corporation, Rockville, Maryland, Document Number TR-15-7, 15 January 1965.

AGC would only reduce this adaptivity and result in design compromises and sub-optimal performance.

Pure pseudo-noise (PN) systems are compared against "hybrid" systems in Sub-section 1.3. The additional power required for the pure PN system is estimated and some of its implementation difficulties are discussed. It is shown that the hybrid system utilizes the available signal power much more effectively than the pure PN system.

The recommendation against the common channel approach is based upon a spectral analysis from which an estimate of the effects of crosstalk upon the operation of an AROD channel is derived. It is shown in Sub-section 1.4 that a common channel system would have a very limited dynamic range over which the AROD accuracy objectives could be met. In addition, the acquisition process would be more difficult with a common channel system. Separation of the four AROD channels substantially increases the dynamic range and eases the acquisition problem.

1.2 LINEAR PROCESSING

The first conclusion to be reviewed is the recommendation that a linear receiver be employed in the spacecraft. In this sub-section, it is shown that by taking advantage of the adaptivity of the phase-lock loop natural frequency, that the linear receiver best suits the wide range of signal dynamics encountered in the AROD system.

In the Fifth Quarterly Report (Volume II, pages B1 through B8), it was shown that the loop natural frequency was a function of the signal amplitude at the input to the phase-lock loop. For a linear receiver (which is defined as a receiver with constant amplification over the range), the signal amplitude is proportional to the range and the loop natural frequency, ω_n, is given by:

$$\omega_n = \sqrt{\frac{A}{A_o}}\ \omega_{n_o} \qquad (1)$$

where

ω_n = loop natural frequency

ω_{n_o} = loop natural frequency at the design point*

A = signal amplitude

A_o = signal amplitude at design point.*

In the case of the limiter receiver, which employs an ideal hard limiter prior to the phase-lock loop, the total power at the output of the limiter is constant. Thus, the signal amplitude at the input to the phase-lock loop is dependent upon the signal-to-noise ratio at the input to the limiter. The loop natural frequency of the limiter receiver is, then, a function of the limiter suppression factor and is given by:

$$\omega_n = \sqrt{\frac{\alpha}{\alpha_o}}\ \omega_{n_o} \tag{2}$$

α = suppression factor

α_o = suppression factor at design point.

In the case of the AGC receiver, the signal level is held at a constant amplitude at the input to the phase-lock loop regardless of the received SNR; thus, the loop natural frequency is constant.

In order to meet the accuracy objectives for the AROD application, there are several conflicting limits imposed on the loop natural frequency. In situations where high doppler rates are encountered (directly overhead, low altitude), the loop natural frequency must be great enough to keep the steady state tracking error of the loop within certain bounds. At maximum range, the loop natural frequency must be small enough to keep the phase error due to thermal noise within certain bounds.

---

* The design point is chosen at the maximum range (4000 nautical miles) for which the system is to operate.

The steady state phase error due to doppler rate is given by:

$$\varphi_{ss} = \frac{D}{\omega_n^2} \tag{3}$$

where

φ_{ss} = steady state phase error per radian

D = doppler rate rad/sec^2

ω_n = loop natural frequency

Thus, for the linear receiver, the steady state phase error is given by:

$$\varphi_{ss} = \left(\frac{A_o}{A}\right)\left(\frac{D}{\omega_{n_o}^2}\right) \tag{4}$$

For the limiter receiver, the steady state phase error is given by:

$$\theta_{ss} = \left(\frac{\alpha_o}{\alpha}\right)\left(\frac{D}{\omega_{n_o}^2}\right) \tag{5}$$

The AGC receiver will have a steady state phase error as given by equation (3).

The phase error due to thermal noise for the linear receiver is given by:

$$\sigma_P^2 = \frac{\omega_{n_o}\,\Phi}{2\zeta_o}\left[\frac{A}{A_o}\,2\zeta_o^2 + \frac{1}{2}\right] \tag{6}$$

For the limiter receiver, the phase error is given by:

$$\sigma_P^2 = \frac{\omega_{n_o}\,\Phi}{2\zeta_o}\left[\frac{\alpha}{\alpha_o}\,2\zeta_o^2 + \frac{1}{2}\right] \tag{7}$$

where

ω_{n_o} = loop natural frequency at design point

ζ_o = loop damping factor at design point

Φ = noise power spectral density to signal power ratio

The loop damping factor at the design point, ζ_o, is chosen as $\frac{1}{\sqrt{2}}$ (for the reasons given in the Fifth Quarterly Report, Volume I, pages 1 through 26). Using this value for the loop damping factor, the thermal phase error at the design point is given by the familiar formula:

$$\sigma_P^2 = \frac{3}{2\sqrt{2}}\ \omega_{n_o}\ \Phi = 1.06\ \omega_{n_o}\ \Phi \qquad (8)$$

The phase error as given in equation (8) would apply to the AGC receiver for all ranges, since ω_n is constant.

In Figure 1-1, the variation of the amplitude ratio $\frac{A}{A_o}$ and suppression factor ratio, $\frac{\alpha}{\alpha_o}$, are plotted versus range. The suppression factor ratio is plotted for two limiters, one with a bandwidth of 0.5 KHz and the other with a bandwidth of 166 Hz. The power in the signal transmitted from the space vehicle was assumed to be 5 watts. As shown, the amplitude ratio has a maximum value of 40 at the 100 mile range, whereas the limiter with the 0.5 MHz bandwidth has a maximum suppression factor ratio value of 7.9 at the 100 mile range. The limiter with the 166 Hz bandwidth has a suppression factor ratio which is approximately 1 throughout the range, as is the case with the AGC receiver. The greater variation of the amplitude ratio $\frac{A}{A_o}$ over the range will result in a loop natural frequency with a greater adaptivity over the range. If, for example, a loop natural frequency of 4 radians per second were chosen at the design point (4000 nautical miles), then the linear receiver phase-lock loop would have a loop natural frequency of 25.3 rad/sec at the 100 mile range, whereas the limiter would only have a 11.3 rad/sec loop natural frequency at this range.

This greater adaptivity of the loop natural frequency in the linear receiver will result in a more optimum receiver, as can be seen in Figure 1-2. In this

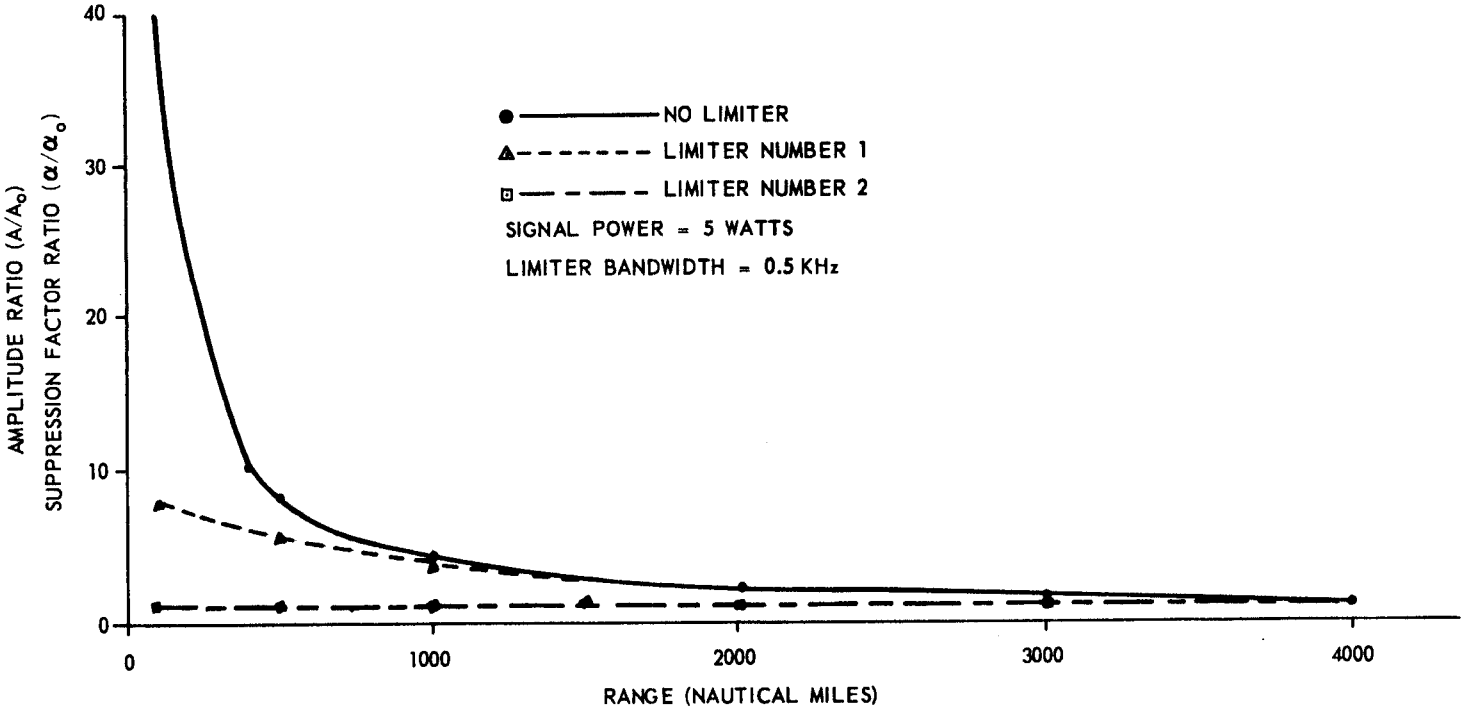

Figure 1-1. Amplitude Ratio and Suppression Factor Ratio Versus Range

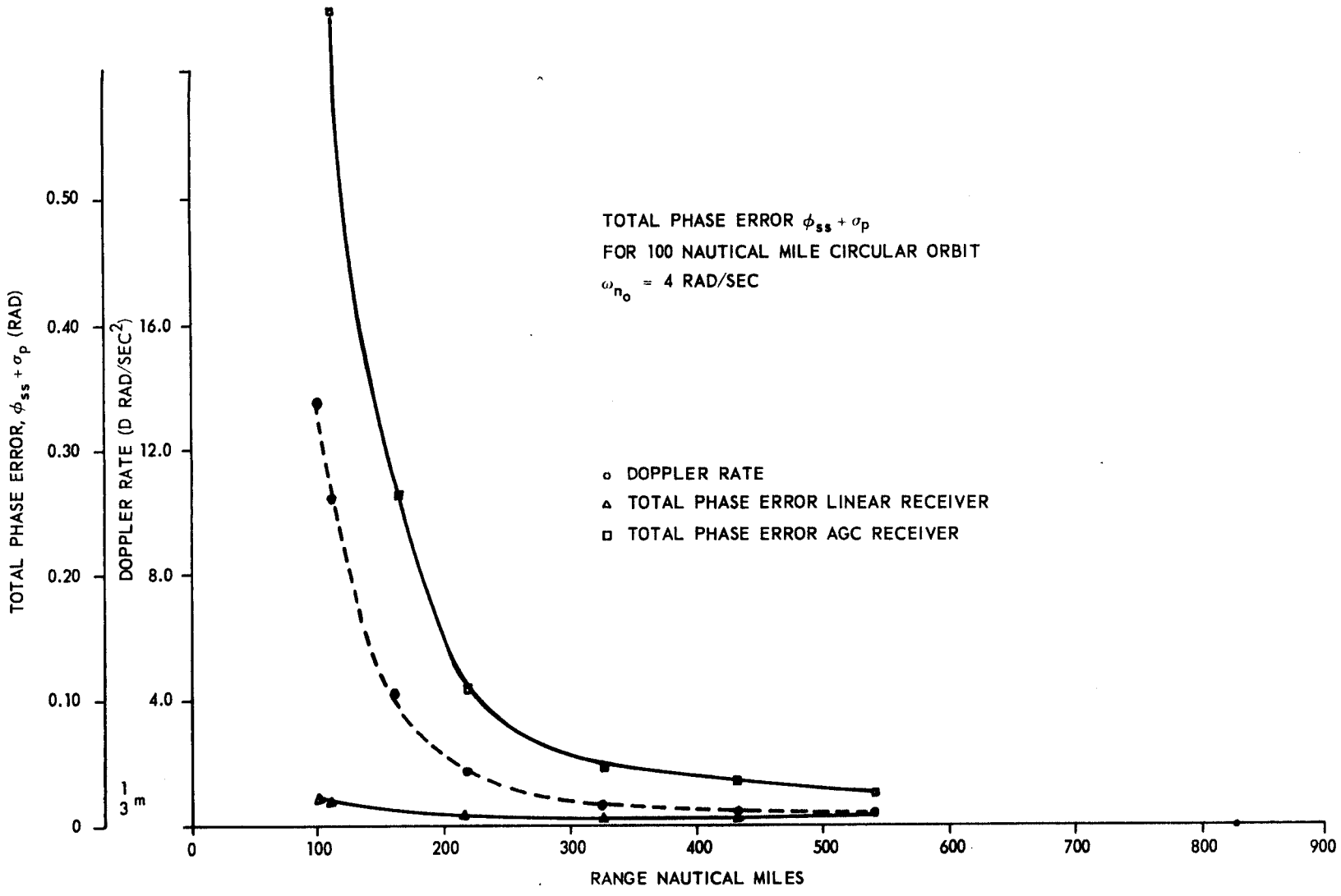

Figure 1-2. Phase Error Versus Range

illustration, the sum of the steady state phase error due to doppler rate and the thermal phase error are plotted for a 100 mile circular orbit. It was assumed that the design point (at the 4000 nautical mile range) loop natural frequency is 4 rad/sec and 5 watts of power is transmitted in the ranging signal from the spacecraft. It can be seen that the phase error in the AGC receiver is much greater than the 1/3 meter objective, whereas the linear receiver is very close to the objective.

The large tracking error of the AGC receiver at short ranges, where the steady-state error is dominant, can be reduced by some means of compensation external to the loop (sometimes termed rate aiding). In general, such compensation is accomplished by sensing the doppler signal and applying an analog of it to the appropriate element in the loop. Of course, the doppler sensing must be accomplished in the presence of the noise that exists in the doppler extraction function for the AROD system. This noise, which will be in part correlated with the noise in the range tracking loop, will degrade the S/N_o at the output of the range tracking loop by 3 db or more, thereby reducing the advantage of the compensation. A further reduction in the effective compensation will result from the transient errors in following the doppler changes. In addition, if compensation in the range tracking loop is accomplished by estimating the doppler signal in the carrier tracking loop, all the gain factors and time constants of the elements of both loops must be stabilized with respect to environmental conditions to a far greater degree than is required for loops which are operated independently. Finally, the steady state errors in the system with rate aiding will be much less predictable since they result from uncertainties in the loop element transfer functions and are random in nature; this will necessitate larger design margins and make post-flight analysis more difficult.

The most significant factor concerning rate aiding is that the amount of compensation that can be effectively achieved in practice could be applied to the linear receiver as well as the AGC receiver. Thus, the linear receiver can always be designated to provide performance superior to that of the AGC receiver. Consequently, the linear receiver is the optimum design for the AROD system.

1.3 HYBRID SYSTEM

The second conclusion to be reviewed is the recommendation for a hybrid system rather than a pure PN system. In this sub-section, a comparison is made between a modulation system employing a pure PN sequence and one employing a periodic signal combined with a PN sequence (a "hybrid" system). The additional power required for the pure PN system is estimated and an example is presented to compare the required tracking filter parameters for both implementations.

The first step in effecting the comparison is to obtain an expression for the range variance for a periodic component tracked by a phase-lock loop. As shown in the preceding sub-section, the phase variance due to receiver noise for a phase-lock loop is given by:

$$\sigma_P^2 = 1.06\, \omega_{n_o} \Phi \tag{9}$$

where

ω_{n_o} = loop natural frequency (rad/sec)

Φ = noise power spectral density to signal power ratio $(\text{cps})^{-1}$

As discussed earlier, ω_n may vary as the received signal power varies, but for the purposes of comparing a pure PN system with a hybrid system, it can be assumed that the variations in ω_n will be the same for both systems.

To convert this phase variance to a range variance, the following transformation is used:

$$R = \left(\frac{\lambda}{2}\right)\left(\frac{\Theta}{2\pi}\right) \tag{10}$$

where

λ = tracking signal wavelength

The variance in the range measurement due to the receiver noise is then

$$\sigma_{r_\varphi}^2 = \left(\frac{\lambda}{4\pi}\right)^2 \sigma_P^2 = \left(\frac{\lambda}{4\pi}\right)^2 \cdot 1.06\, \omega_{n_o} \Phi \tag{11}$$

To complete the desired comparison, a method to determine the range variance when a pure PN system is employed must be known. The time delay variance for a PN sequence, as derived by Spilker [1], is given by:

$$\sigma_t^2 = 2.12\ \Delta^2 \left(\frac{M}{M+1}\right) \frac{N_o' \omega_{n_o}}{P_s} \tag{12}$$

where

Δ = bit duration

M = number of bits in sequence

N_o' = double-sided noise power spectral density

ω_{n_o} = loop natural frequency

P_s = signal power

In this expression, it is assumed that $\zeta = \frac{1}{\sqrt{2}}$ and that the PN sequence is tracked by a delay lock discriminator. If it is assumed that M is large and we convert to the single-sided noise power spectral density (rather than the double-sided) the following obtained:

$$\sigma_t^2 \approx 1.06\ \Delta^2\ \frac{N_o \omega_{n_o}}{P_s} \tag{13}$$

Again, converting to the range variance, this time using the transformation:

$$R = \frac{ct}{2} \tag{14}$$

where

c = velocity of light.

---

(1) J. J. Spilker, "Delay-Lock Tracking of Binary Signals," IRE Transactions on Space Electronics and Telemetry, March 1963, pp. 1 through 8.

The one-way range variance is then

$$\sigma_{r_d}^2 = \left(\frac{c}{2}\right)^2 \sigma_t^2 = \left(\frac{c}{2}\right)^2 1.06\,\Delta^2 \frac{N_o\,\omega_{n_o}}{P_s} \tag{15}$$

$$\sigma_{r_d}^2 = \left(\frac{c\,\Delta}{2}\right)^2 1.06\,\omega_{n_o}\,\Phi \tag{16}$$

To compare the power requirements of the PN sequence to those for the hybrid system, the range variances for the two systems are equated to obtain:

$$\frac{P_s}{S} = (2\pi)^2 \left(\frac{c\,\Delta}{\lambda}\right)^2 \tag{17}$$

where

S = signal power for the phase-lock loop

Letting

$f_T = \frac{1}{T}$ = frequency of signal in phase-lock loop

$f_\Delta = \frac{1}{\Delta}$ = bit rate of pseudo-noise sequence,

the ratio of the power required for the PN sequence to that for the hybrid system (phase-lock loop) becomes:

$$\frac{P_s}{S} = (2\pi)^2 \left(\frac{f_T}{f_\Delta}\right)^2 \tag{18}$$

In Figure 1-3, the ratio of delay-lock discriminator signal power to phase-lock loop signal power is plotted versus the ratio of tone frequency to PN bit rate. As shown, in order to achieve the same accuracy as a phase-lock tone with equal power, the bit rate of the pseudo-noise sequence must be 6.28 times the tone frequency.

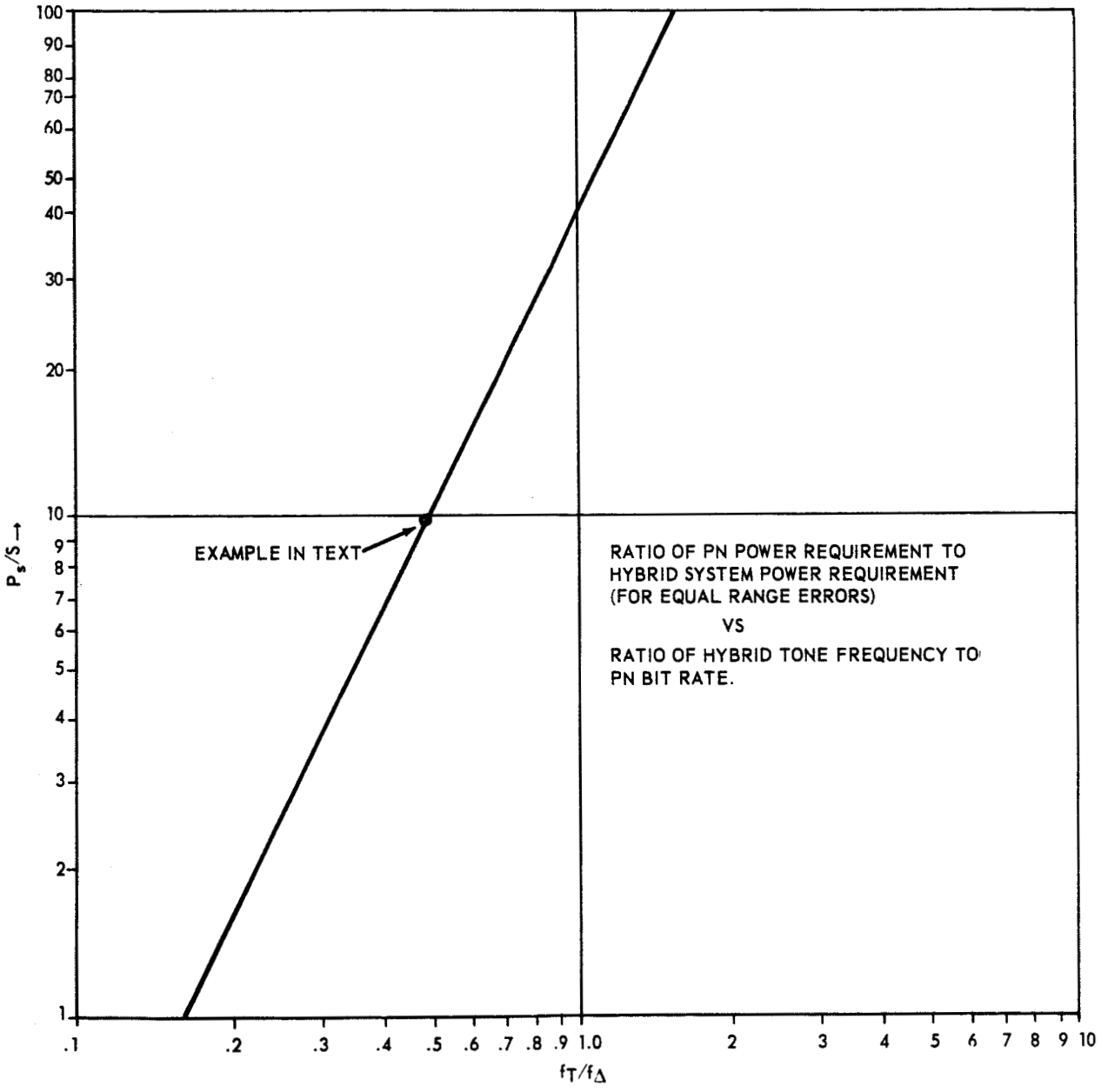

Figure 1-3. Comparison of Power Requirements for Pure PN System (P_s) and Hybrid System (S)

Many additional comparisons could be made to demonstrate the advantages of the hybrid system over the pure PN system. For any specific permutations of parameters, the relative requirements can be determined by comparing equations (11) and (16).

As an example, consider the range accuracy requirements (1σ) of 1/3 meter (specified on page 1-6 of the Fifth Quarterly Report) and determine the implementations necessary to achieve this accuracy at the maximum range of 4000 nautical miles. For separate channels,* a reasonable assumption for the PN bit rate is 1.6 Mbps; this results in a separation of 3.2 MHz between the spectrum null just below the carrier frequency and the null just above the carrier frequency. For the hybrid system, a reasonable assumption is that the periodic component has a frequency of 800 KHz and that the hybrid modulation waveform is identical to that described on pages C-12 and 13 of Volume II of the Fifth Quarterly Report; this, again, results in spectral nulls located at 1.6 MHz above and below the carrier frequency. Assuming that $\Phi = 1/20,000$ $(\text{cps})^{-1}$ at 4000 nautical miles, and solving equation (11) for ω_{n_o}, it is found that the loop natural frequency required for the phase-lock loop is approximately 2.4 radians/second. To compare this with the requirements for the pure PN system, equation (16) is solved for ω_{n_o}, and it is found that a loop natural frequency of 0.25 radians/second is required.

Thus, it is shown that the tracking filter for the pure PN system will be considerably more difficult to implement. In addition, much more rate aiding must be provided with the smaller ω_{n_o} in order to track the high doppler and doppler rate situations.

1.4 COMMON CHANNEL EVALUATION

In this sub-section, the justification is presented for the third major conclusion — the recommendation against common channel operation. The presentation centers upon the dynamic range limitations encountered with

---

* Separate channels are assumed for this example (rather than common channel operation) in accordance with the recommendation contained in Sub-section 1.4; a similar example for a common channel implementation would yield the same relative results.

common channel operation; acquisition problems with common channel operation are also discussed.

1.4.1 Dynamic Range Analysis

The necessity for the AROD system to operate over a wide dynamic range is one of the most important considerations in the selection of the modulation waveforms. Because of range differences, multipath effects, propagation anomalies, and so on, the spacecraft receiver must have the capability to simultaneously process signals that differ markedly in their relative strengths. The objective for this dynamic range capability, as given in the RFP for the AROD System Test Model Hardware,* is 70 db. Hence, dynamic range becomes an extremely important evaluation criterion for comparing candidate modulation techniques for the AROD application. Modulation systems which have superior dynamic range performance and which maintain a good balance between crosstalk and thermal noise errors should be given first consideration.

To compare a common channel system** with one employing four separate channels, it is necessary to examine the spectrum for a PN sequence under the usual approximations: this is the $(\sin^2 x)/x^2$ envelope shown in Figure 1-4.

In this illustration, it is shown that the first sidelobe is 13 db below the main peak. Thus, the crosstalk introduced into an adjacent channel in a system using separated channels is at least 13 db less than the crosstalk encountered in a common channel system. Filtering each separate channel would significantly reduce the sidelobes (crosstalk), and increase the dynamic range for the separate channels, but not for the common channel approach. Since the ratio of the main peak to the sidelobes (suppressed) represents the dynamic range advantage of the separate channels over the common channel system, it is apparent that separate channels will provide substantially more dynamic range.

---

* RFP No. 1-4-40-01283, NASA Marshall Space Flight Center, Huntsville, Ala.

** Common channel operation refers to the case in which each of the four AROD channels occupies essentially the same frequency band.

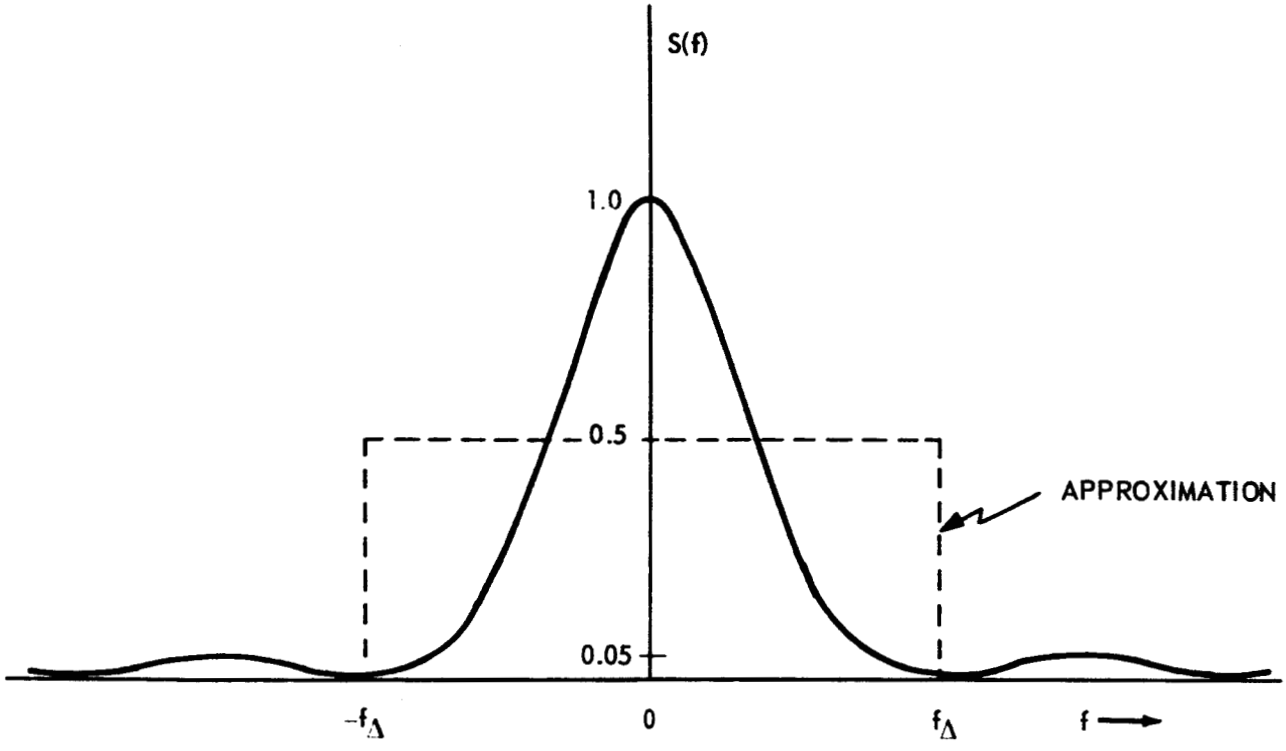

Figure 1-4. Envelope of Received PN Power Spectral Density

As the next step in the evaluation of the common channel approach, an estimate of its dynamic range is now presented. To accomplish this, it is necessary to approximate the true spectrum with the dotted rectangle shown in Figure 1-4. This approximation, which is commonly employed, is equivalent to assuming that the received modulated signal of another channel is white Gaussian noise as far as the channel of interest is concerned;* that is, the power received for one channel is assumed to be spread over a bandwidth $2f_\Delta$, or twice the PN sequence bit rate. Hence, the effective noise spectral density produced by the undesired channel is $YS/2f_\Delta$, where S is the power in the desired signal and Y is the ratio of the undesired power to the desired signal power.

The most useful method for estimating the dynamic range is to calculate the value of Y which causes measurement errors equivalent to those caused by thermal noise at the maximum range (that is, $\sigma_r \approx \frac{1}{3}m$, $\sigma_{\dot{r}} \approx .01$ m/sec). This value of Y is obtained from:

$$\frac{Y_{crit}}{2f_\Delta} = \Phi_{max}$$

where Φ_{max} is the maximum value of Φ, the noise-power-density-to-signal-power ratio $(cps)^{-1}$. Assuming that $\Phi = 1/20,000\ (cps)^{-1}$ and $f_\Delta = 6.4$ Mbps, the result is Y = 28 db.

The implication is clear. A common channel system will only have dynamic range of approximately 28 db.

If, for example, the undesired power were 40 db greater than the desired signal, measurement errors four times greater than the AROD objectives would occur.

As to the question of the validity of the approximation shown in Figure 1-4, this approximation, if anything, must be optimistic in terms of the crosstalk effects actually encountered. The actual spectrum contains discrete components which may result in partial correlations in the tracking filters, thereby causing

---

* The validity of this approximation is discussed later.

larger errors than true white noise. Thus, the conclusion that the dynamic range of the common channel approach is very limited is furthered strengthened.

1.4.2 Acquisition Analysis

The acquisition of the PN modulation in the presence of strong interference from another channel will be much more difficult than without this interference. Even if it is assumed that the carrier loop is locked in, it will still be necessary to correlate the incoming signal with the slave PN generator for a longer time in the common channel system. The basic factor determining acquisition performance is E/N_o. The larger the E/N_o, the greater the probability of detection and the smaller the probability of false alarm. Therefore, the increased effective N_o present in the common channel approach necessitates an increase in correlation time to preserve the same E/N_o and the same acquisition performance as the separate channels provide.

The higher bit rate will, of course, also make acquisition more difficult for the common channel approach.

1.4.3 Summary

Because of the stringent specifications for the AROD system, dynamic range must be considered an extremely important criterion in the evaluation of candidate modulation techniques. It has been shown that separate channels have consistently better performance in this respect than a common channel system; the dynamic range for the latter has been estimated to be only 28 db. Moreover, the use of a common channel system will cause acquisition and reacquisition to be more complex and time-consuming.

For these reasons, it is recommended that separate channels be used in the AROD system.

Section 2

PHASE-LOCK LOOP ADVANCED CIRCUIT INVESTIGATIONS

2.1 DESIGN APPROACH FOR MEMORY AIDED PHASE-LOCK LOOP

In the Fifth Quarterly Report*, a technique of exploiting new developments in field effect semiconductor devices, to permit the implementation of analog storage, was described. A controllable, reproducible analog storage (memory) was shown to permit unaided acquisition for a loop when incorporated as proposed. It was shown that, not only doppler offset, but also doppler rate has a great impact on the acquisition and reacquisition capabilities of the loop, so that perfect memory of doppler offset (such as might be afforded by an ideal Type II loop) at signal drop-out alone is insufficient. Several system approaches were advanced as a solution to the storage of both of these analog signal parameters. The most advantageous to implement uses a single analog storage circuit which continuously monitors the phase detector (loop multiplier) output while tracking a signal. The single analog storage circuit supplies a synthesized signal containing both doppler offset and doppler rate elements to the loop upon loss of signal; this provides the Voltage Controlled Oscillator with a control which maintains its frequency to the estimated frequency of the signal. It was also pointed out that, upon reappearance of the signal, the control signal from the memory circuit should continue until relock is achieved to improve the signal capture capabilities. It was suggested that search can be accomplished and implemented, which is initiated after a suitable wait-on-memory period, allowing for a temporary signal fade. A Mode Detector is required to sense the condition of the loop — tracking a signal, signal present in proximity, or no signal present. The Mode Detector controls several analog signal gates to accomplish the various loop functions.

---

* Special AROD System Studies, Fifth Quarterly Report, International Business Machines Corporation, Rockville, Maryland, Document Number TR-15-7, 15 January, 1965.

The suggested design approach has been verified by a breadboard construction of all the necessary loop and control components and by initial tests on the loop tracking, memory, and acquisition behavior. The engineering model Type I phase-lock loop will have a suitably constructed analog storage element incorporated in it for performance testing.

In the forthcoming period, construction of an engineering model of the phase-lock loop and its associated memory circuit will be completed. In addition, the mode detector and control circuits will be redesigned and constructed. The loop capabilities of acquisition on search, tracking of a signal, memory, and reacquisition on signal fade can then be verified.

2.2 DESIGN CONSIDERATIONS

As outlined in Section 1 of the Fifth Quarterly Report, several constraining factors determine the parameters of the phase-lock loop. To obtain the specified system accuracy for a high doppler offset, a minimum loop gain must be maintained, while the required signal-to-noise ratio determines the loop bandwidth. The use of a signal dependent, variable gain loop multiplier allows the loop to adapt to changing signal conditions.

For the construction of an engineering model of a memory-aided phase-lock loop, use will be made of the presently available Loop Voltage Controlled Oscillator and Loop Multiplier (described in the Fourth Quarterly Report) supplemented by a Loop Filter and amplifier. The Loop Multiplier changes its gain by a factor of 10 from minimum to maximum signal-to-noise ratio. To meet the various system requirements, the loop parameters can be calculated and are listed in Table 2-1.

In addition to the basic phase-lock components, additional circuitry is required to obtain the desired analog memory, gating, mode detection, and search functions. A block diagram of the complete loop is shown in Figure 2-1. The incoming signal is limited in the stage preceding the Loop Phase Detector, where it is multiplied with the output of the VCO. The Phase Detector output is applied to the Loop Filter, and after amplification, applied to the VCO to control its frequency and phase. When the loop is locked to a signal, gate A

Table 2-1

Parameters of Memory-Aided Phase-Lock Loop
(Carrier Tracking Filter Case)

Parameter	Symbol	Min SNR	Max SNR
Gain	k	1.5×10^6	1.5×10^7
Lag time constant	τ'	150	150 sec
Natural frequency	ω_n	100	316 rad/sec
Damping factor	ζ	0.707	2.24
Two-sided bandwidth	2B	106	525 Hz
Lead time constant	τ	14.1	14.1 msec

is open, while gates B and C are closed. These gates are implemented by MOSFET (metal oxide semiconductor field effect transistor) devices (a brief description of these devices is given in Appendix A). The Memory Unit input is gated to the signal at the Phase Detector output through a low pass filter and follows this signal in normal loop operation (tracking).

In a loss-of-signal condition, A is closed and B is opened immediately, while gate C is held closed for an arbitrary amount of time, in which the signal is allowed to reappear. In the present design, this time delay is set at 8 seconds to facilitate testing of the memory function. During this time, at which the Loop Phase Detector output contains no signal information, the VCO frequency is slewed under the control of the last doppler offset and last doppler rate, which are synthesized by the Memory Unit. Since the Loop Filter/Amplifier is driven from a voltage source during this mode, a decay in doppler rate compensation occurs. However, with the 150 second time constant of the loop, the rate compensation decay in a 1.5 second dropout is only 1 percent. The doppler offset memory is not affected.

If the signal reappears within the 8-second search-delay time interval and falls within a frequency band which guarantees a fast reacquisition, the

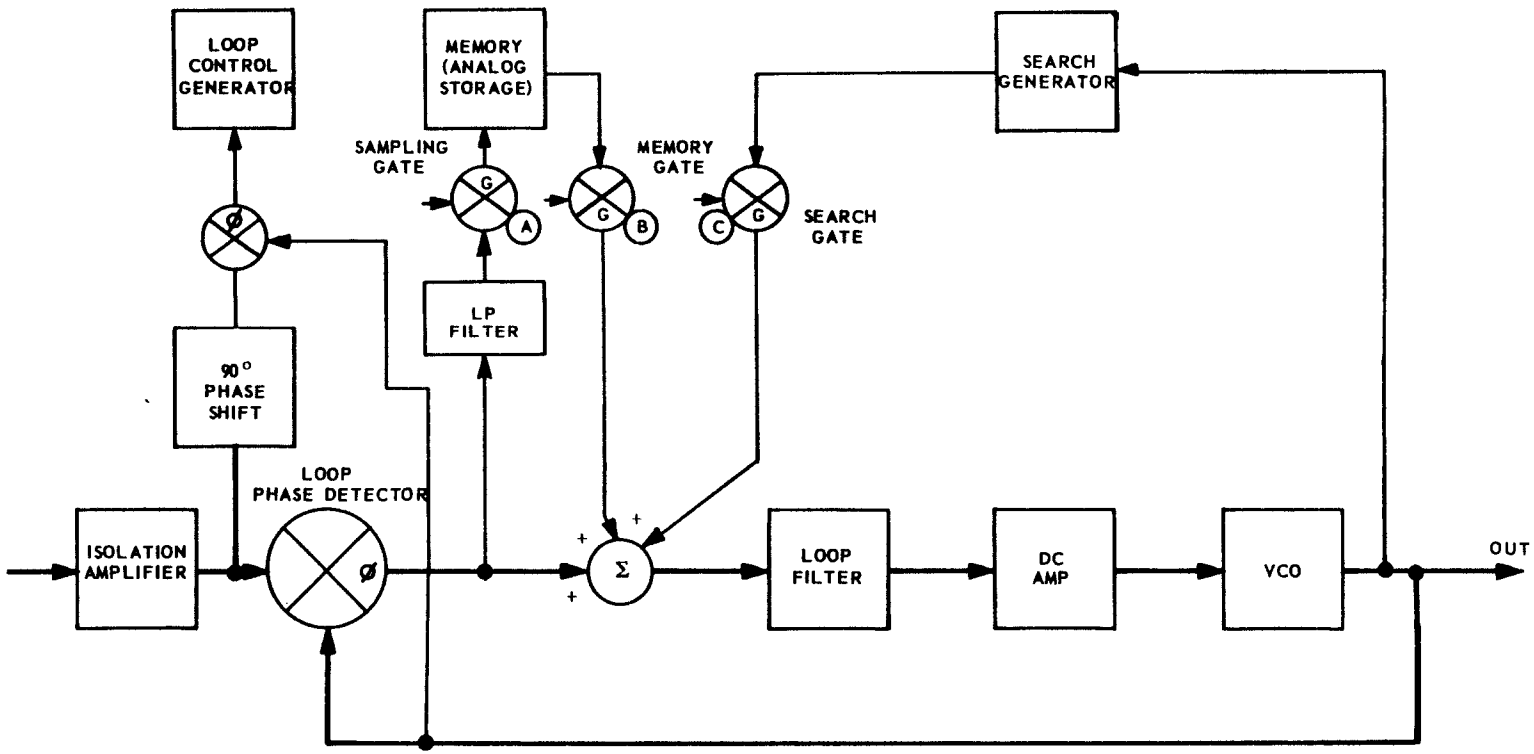

Figure 2-1. Block Diagram of Memory-Aided Phase-Locked Loop

search-delay timer is disabled, and the Memory Unit continues to steer the VCO in order to enhance pull-in and lock capabilities while the output of the Loop Phase Detector contains the required pull-in signal. If the signal does not fall in this detectable frequency band, lock can still be accomplished, provided it is achieved before the total 8-second delay. Upon lock, gate A is reclosed to sample the revised doppler signal, while gate B is reopened to allow normal loop operation. The information supplied by the output of the Memory Unit to the loop is then immediately replaced by a voltage from the Phase Detector by means of a small slippage or advance of phase of the VCO signal.

If, however, the signal has not reappeared within the 8-second search-delay period, or reappears out of range, gate C will open and insert a search voltage to the loop, which slews the frequency of the VCO through the expected signal range at a very fast rate in a near linear fashion. At a pre-determined frequency, established by monitoring the Loop DC Amplifier output, the direction of search is reversed and continued, at the same rate, to the other end of the search range, resulting in a triangular search. In the present system, a 200 KHz range is searched in 10 seconds. The search is discontinued when a signal appears in the detectable acquisition band, and acquisition is accomplished as previously described.

Referring to Figure 2-1, the search voltage is applied to the summing point of the loop; consequently, removal of search may cause a reversal of the change in VCO frequency, preventing lock-on, since the previous doppler information is still duplicated. To prevent this condition, the acceptable frequency band in the search control circuit must be narrow so that the search is only discontinued when the frequency of the VCO is very close to that of the signal. This is in agreement with the detectability requirement of a signal in noise. A 2 millisecond low-pass filter will guarantee a beat frequency of less than 100 Hz, particularly since in the 2 millisecond charge time, the VCO is swept by the search circuit at a rate 80 Hz above that previously mentioned. In addition, this bandwidth of search-cutoff is dependent on signal strength as the phase detector gain changes, and adaptively increases this bandwidth for a stronger signal.

Other forms of search, such as those with an additional sine wave voltage applied to simulate doppler rate, as described in the Fifth Quarterly Report, were not investigated.

To perform the various gating and control functions, a Mode Detector is required which senses the condition of the loop and triggers some control circuits and time delays operating on the principle loop components. Sensing is achieved simply by shifting an External Phase Detector 90 degrees from the Loop Phase Detector. When the loop is locked, the output of the External Phase Detector is a DC voltage; when a signal is close, it is an AC voltage; and in the absence of a signal, the output is zero. In the presence of noise at the loop input, the detector output is disturbed by noise, which establishes a limit to the frequency of a detectable AC signal voltage. With a 2 millisecond (> 100 Hz) bandwidth, the signal-to-noise ratio is always in excess of 20 db. The output of this detector is used to operate the various control circuits.

2.3 MEMORY-AIDING IMPLEMENTATION

2.3.1 Loop Filter and DC Amplifier

The required gain and time constants listed in Table 2-1 determine the design characteristics of the Loop Filter and DC Amplifier. With the values given for the other loop components, the DC gain should be 100 x, the lag time constant 150 seconds, and the lead time constant 14.1 milliseconds. A time constant of 150 seconds is difficult to obtain when using a reasonably sized capacitor, unless operational amplifier techniques are used. Tantalum capacitors, normally used if high capacitance values are required, have a relatively high leakage current which are dependent upon temperature. In the present design, feedback techniques effectively multiply the capacitance of the feedback capacitor by the open loop amplification. This, however, puts a limitation on the feedback element leakage permissible around the amplifier. This problem has been eliminated by the use of MOSFET devices which exhibit an extremely high input-output isolation.

Figure 2-2 is a schematic of the Loop Filter and Amplifier. The Amplifier input consists of a 2N3609, a dual MOSFET device packaged in a modified TO-5

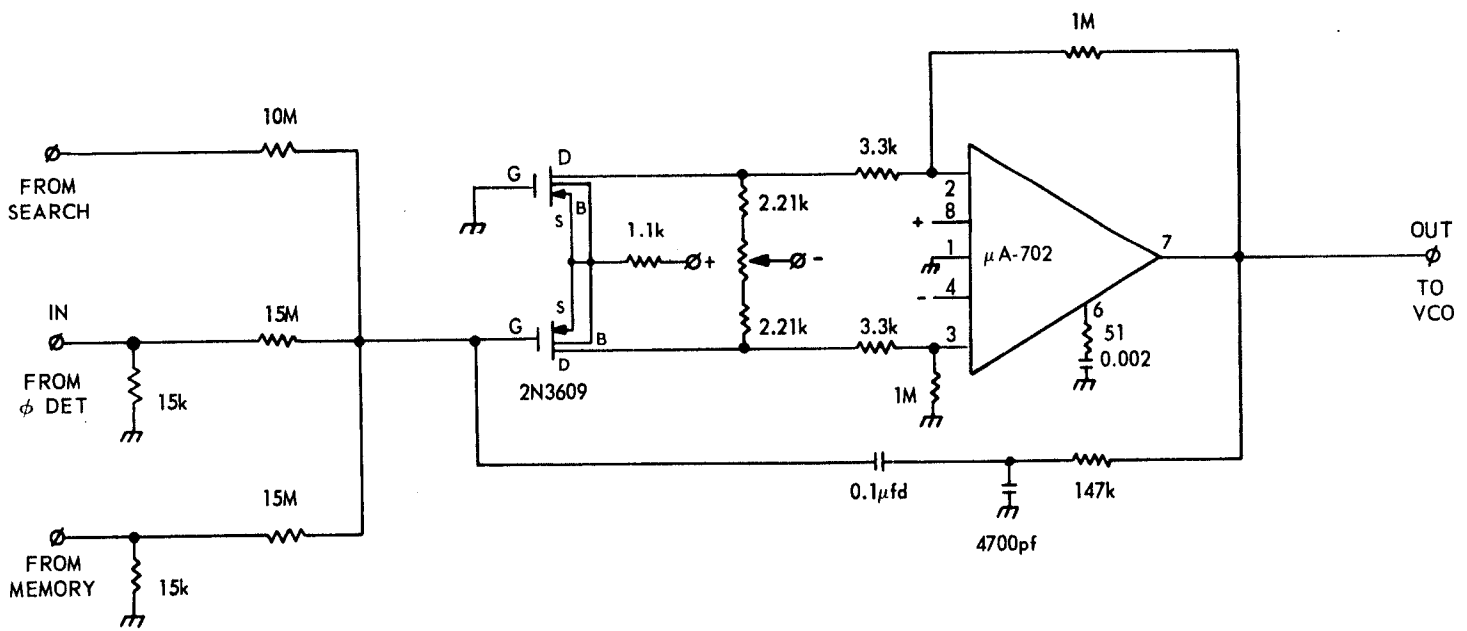

Figure 2-2. Loop Filter and Amplifier

can. It presents, essentially, an infinite input impedance, and provides a balanced drive signal to the operational amplifier. The operational amplifier, a Fairchild μA-702 linear, integrated wideband DC amplifier, also packaged in a modified TO-5 can, supplies an additional gain which is fixed by a DC feedback configuration. The overall closed loop DC gain of the balanced input and the integrated amplifier stages is 200, allowing for a loss of a factor of 2 in the filter circuitry.

A low leakage 0.1 μF storage capacitor, in series with a 147 kilohm resistor, is connected between the output and the input of the amplifier. A 15 megohm input summing resistance completes the required Loop Filter. A second input is required to control the loop in the memory mode, which is also connected to the amplifier input through a 15 megohm resistance. Since the effective value of the feedback capacitor and resistor is raised by the factor of amplification (200), the lag time constant τ' is $200 \times 10^{-7} \times 15 \times 10^{6} \times 0.5 = 150$ seconds, while the lead time constant τ is $10^{-7} \times 147 \times 10^{+3} = 14.7 \times 10^{-3}$ seconds. A balance control is provided to compensate for any differential gain between the two MOSFET devices, while a frequency compensation network is connected to the integrated amplifier. A third input is provided to allow for the search mode of the loop. The equivalent circuit of the loop amplifier and filter is shown in Figure 2-3.

2.3.2 Loop Memory

The design goals for the Loop Memory analog storage circuit are unity gain amplification during track mode, and a near infinite non-volatile hold during the memory mode. The basic circuit configuration used is shown in Figure 2-4. With the gate open, the circuit is essentially an inverting unity gain amplifier with some filtering action provided by the feedback capacitor. When the gate closes, the charge on the capacitor cannot leak off, and continues to maintain the output voltage by control of the amplifier input, providing the input impedance is extremely high. This condition is met by the use of a MOSFET as the input stage of the amplifier.

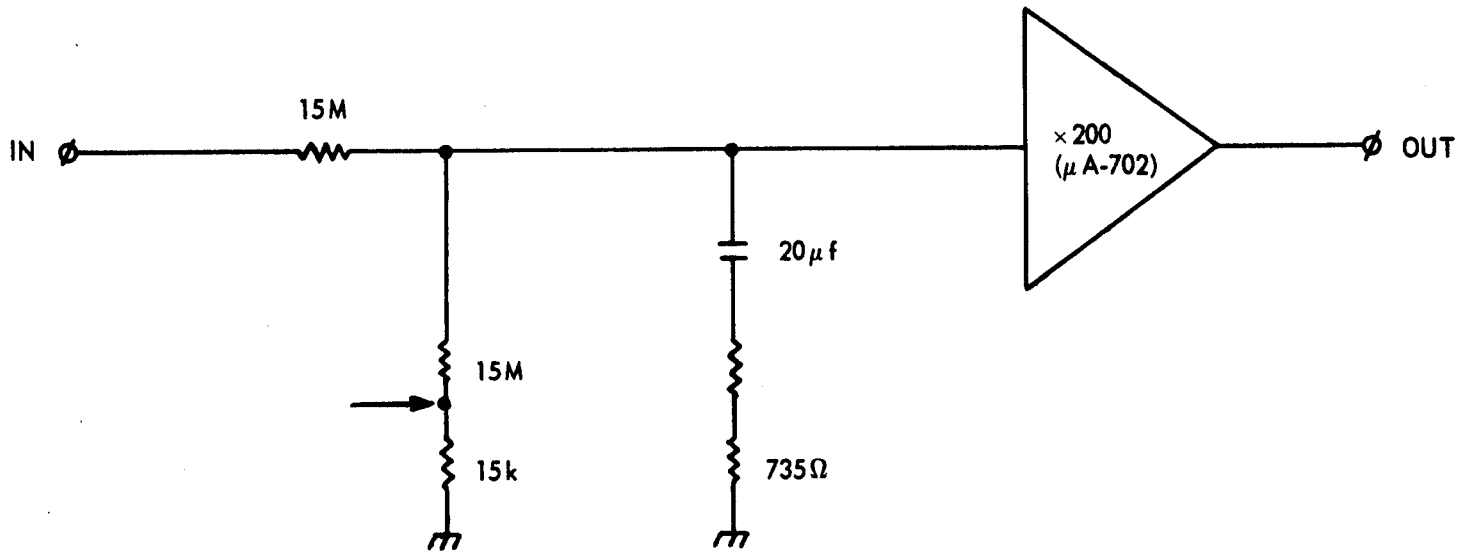

Figure 2-3. Loop Filter and Amplifier Equivalent Circuit

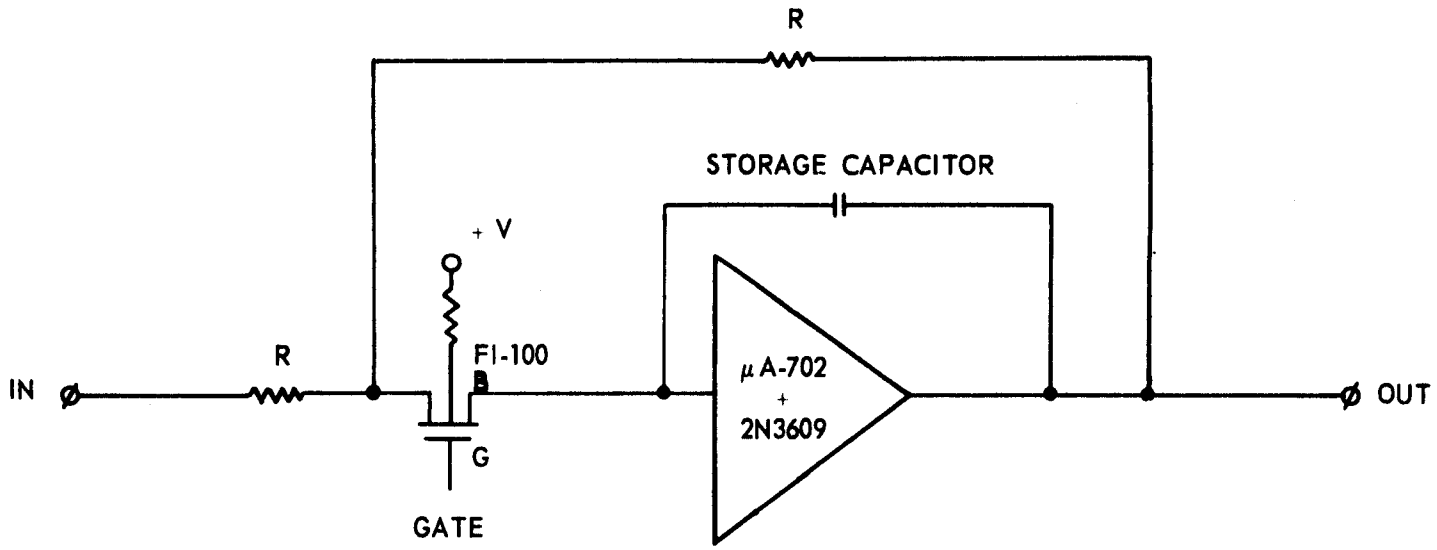

Figure 2-4. Loop Memory, Basic Circuit Configuration

The basic circuit has two drawbacks. It provides a -1 instead of +1 amplification, and, since signal levels at this point in the loop are low, balance and drift of the input MOSFET becomes important. Both problems can be overcome by the addition of a preamplifier, which reduces the effect of drift and provides an additional phase reversal. The gain of the memory amplifier has to be reduced by the same amount to obtain an overall unity gain.

The complete schematic of the Loop Memory unit is shown in Figure 2-5. The preamplifier, using a μA-702 linear integrated DC amplifier, provides a gain of about 20, while some filtering of the incoming noise is achieved by the addition of a feedback capacitor. It is followed by a MOSFET switch, which is used as a sample gate (gate A in Figure 2-1) and an operational amplifier with a loss identical to the preamplifier gain, connected in a configuration similar to that used for the Loop Amplifier. The feedback capacitor is a high quality, low leakage type, and serves as the analog storage element. The output gain (gate B in Figure 2-1) is used to insert the memory output into the loop when required. Resistors are inserted in the connections to the MOSFET gates to minimize the chance of accidental damage.

Initial tests have determined that the time constant of the memory unit is in the order of a "weekend" (about 200,000 seconds), well in excess of the 150 second loop time constant. The operation of the memory unit in conjunction with the loop gave expected results on signal drop-out. Performance evaluation on the complete engineering model remains to be accomplished.

2.3.3 Mode Detector and Loop Control

For functional testing of the phase-lock loop and its associated memory and search circuits, a detector and control circuit have been breadboarded. The circuits are shown in Figure 2-6, but will be redesigned to allow for testing with low signal-to-noise ratios.

The phase detector, identical to that used for the Loop Phase Detector, is preceded by a 90 degree phase shifter. The output of the Mode Detector is connected to a two-stage gate control circuit which, upon either a presence or absence of a phase-lock condition, switches the loop gate into the required

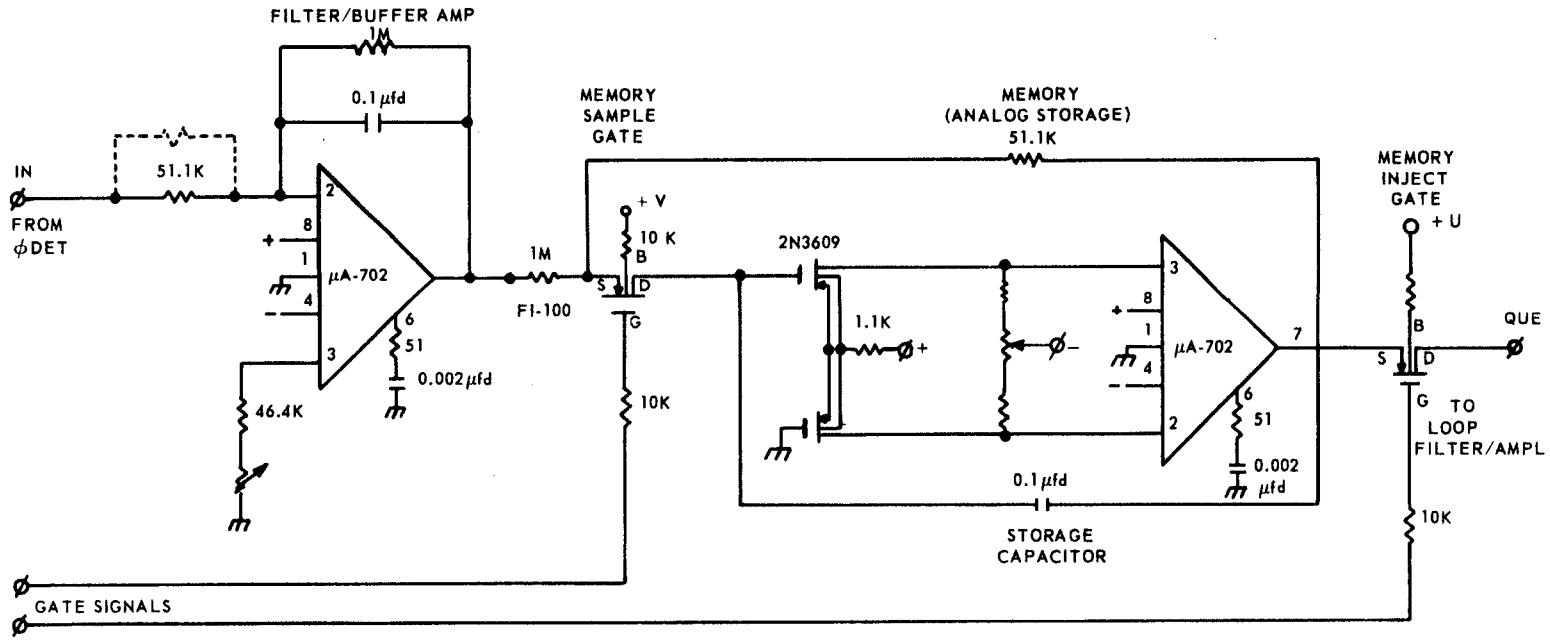

Figure 2-5. Loop Memory, Schematic

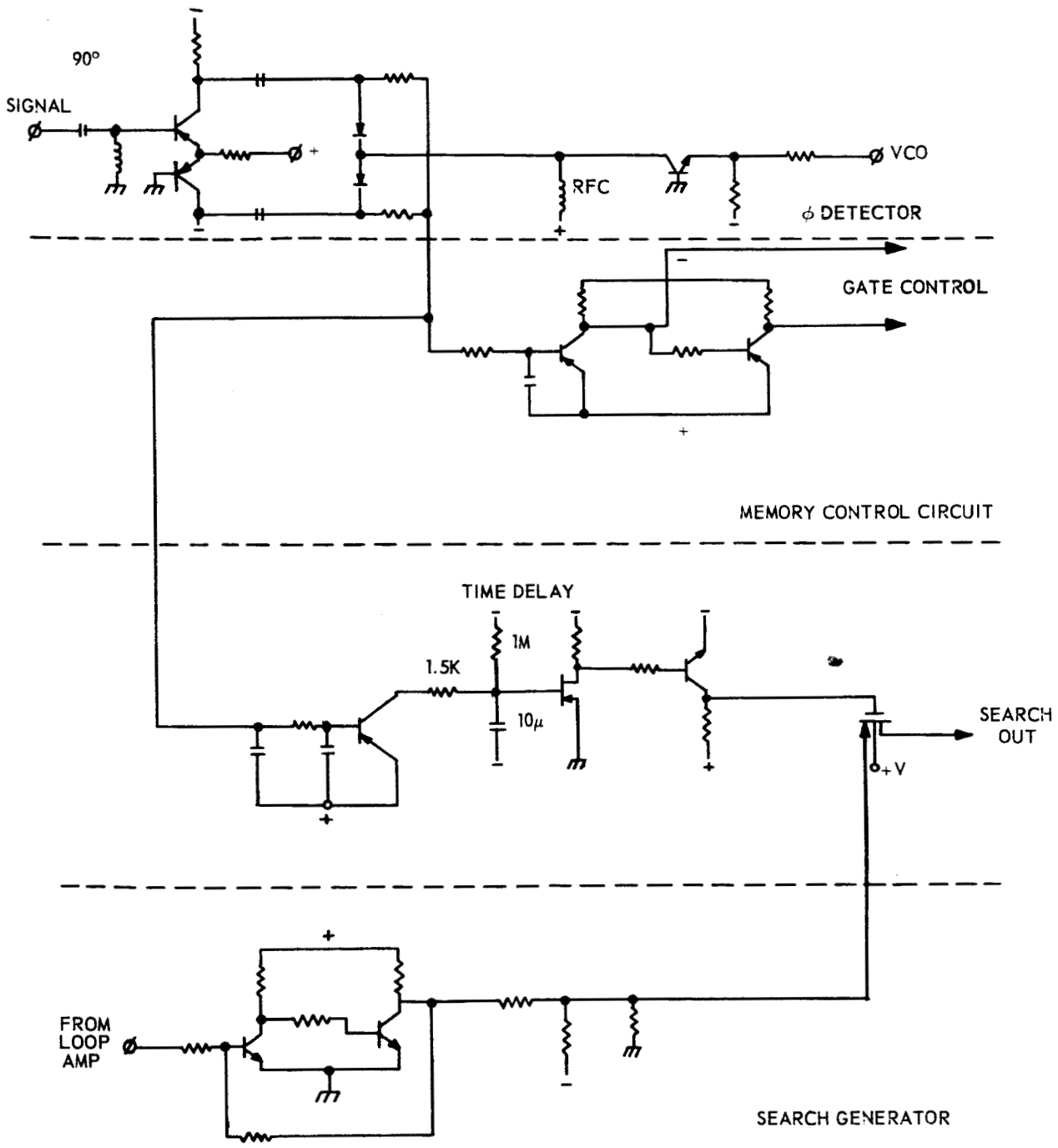

Figure 2-6. Mode Detector and Loop Controls

condition. Additionally, the output is connected to an "AC" detector which operates an 8-second timer. This timer, in turn, controls a MOSFET gate (gate C in Figure 2-1) to connect a search voltage to the loop in the absence of the signal. A bi-stable circuit controled by the output of the Loop Amplifier provides the search function.

Section 3

SPECTRUM AND REACQUISITION ANALYSES

This section discusses the work performed on the Wideband Modulation Techniques task, during the past quarter in the areas of spectrum analysis (Subsection 3.1) and reacquisition techniques (Sub-section 3.2). The spectrum analysis includes generalized equations resulting from the modulation of a carrier with filtered PN signals, and discusses potentially useful approximations to these equations. In the reacquisition techniques investigation it is shown that reacquisition times of less than 1/2 second can be achieved on PN (or hybrid) signals designed for AROD with straightforward implementations.

3.1 SPECTRUM ANALYSIS

3.1.1 Introduction

In the range and range rate tracking system in which a pseudo-noise sequence is used for the range modulation, the carrier may be either bi-phase modulated or phase modulated by the pseudo-noise sequence. If the waveform of the pseudo-noise sequence is ideal, that is, instantaneous change of states, then for a $\pm \pi/2$ (or 0 to π) bi-phase modulation or phase modulation, the power spectrums are identical. However, when non-ideal waveforms are used, that is, waveforms with discrete rise and fall times, then the bi-phase modulation will cause an amplitude modulation of the carrier. The use of phase modulation results in a constant envelope signal; however, the analytic solution for the resulting rf spectrum is not easily obtained. The calculation of the rf spectrum becomes necessary when it is required that the spectrum outside a certain bandwidth meet certain requirements. Also, it might be desirable to compare the spectrum when frequency rather than phase modulation is used.

Several methods of calculating the rf spectrum for angle modulation by filtered pseudo-noise sequences are given in this section. Each of the methods makes certain assumptions which may not fit the physical situation, and both methods require the use of a digital computer to obtain a plot of the spectral density. It would, therefore, be appropriate to obtain an analog solution to the problem by use of a power spectrum analyzer in order to choose the best model to be used. The first method replaces the power spectra of the PN sequence with a gaussian process with the same spectral density; the second method replaces the PN sequence with a sum of independent cosine (or sine) waves, each with uniform independent phase distribution which has the same power spectral density as the PN sequence. The resulting expression for the rf spectrum will require a digital computer to give a useable result.

3.1.2 Gaussian Equivalent

In the guassian equivalent method, the power spectral density of the pseudo-noise sequence is assumed to be that of a gaussian random process; then the power spectral density of the carrier angle modulated by this process can be found.

Let the carrier with the angle modulation by the pseudo-noise sequence be given by:

$$y(t) = \cos(\omega_c t + x(t) + \theta) \tag{19}$$

where x(t) is the pseudo-noise sequence, which for the present is assumed to be ideal, and θ is uniformly distributed between 0 and 2π.

The pseudo-noise sequence is assumed to be a maximal length sequence in which the period of the sequence is denoted by p . That is:

$$p = 2^n - 1 \tag{20}$$

where

n = number of bits in shift register.

Let t_o be the duration of one bit of the pseudo-noise sequence; then the total duration of the sequence is pt_o. The autocorrelation function of the

pseudo-noise sequence is shown in Figure 3-1. The power spectral density of the pseudo-noise sequence is then given by:

$$S_x(f) = \frac{p+1}{p^2}\left(\frac{\sin\left(\frac{\omega t_o}{2}\right)}{\left(\frac{\omega t_o}{2}\right)}\right)^2 \sum_{\substack{n=-\infty \\ n\neq o}}^{\infty} \delta\left(\omega - \frac{2\pi n}{pt_o}\right) + \frac{1}{p^2}\delta(\omega) \qquad (21)$$

The autocorrelation function of the pseudo-noise sequence can then be written as

$$R(\tau) = b_o + \sum_{i=1}^{\infty} b_i \cos\lambda_i \tau \qquad (22)$$

where

b_i is the average power in each harmonic and $\lambda_i = \frac{2\pi i}{pt_o}$.

Now, if the term b_o is neglected, which is the power in the DC component, it can be seen that

$$b_i = 2\left(\frac{1+\frac{1}{p}}{p}\right)\left(\frac{\sin\frac{\pi i}{p}}{\frac{\pi i}{p}}\right)^2 \qquad (23)$$

$i = 1, 2 \ldots .$

If the DC term is neglected the process given by:

$$x(t) = \sum_{i=1}^{\infty} (\eta_i \cos\lambda_i t + \zeta_i \sin\lambda_i t) \qquad (24)$$

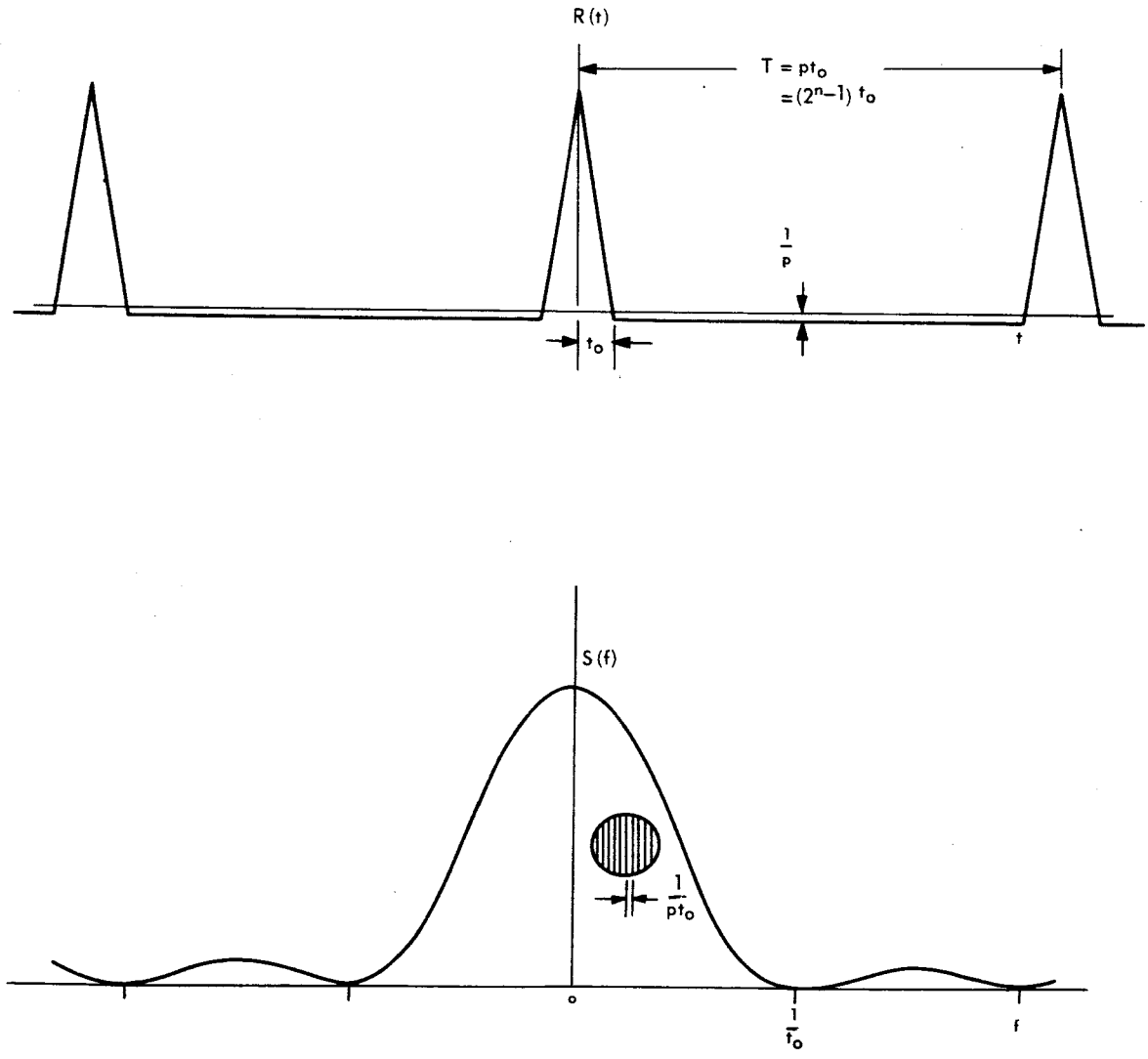

Figure 3-1. Autocorrelation Function and Power Spectral Density of Psuedo-Noise Sequence

in which η_i and ζ_i are gaussian random variables, and the following conditions hold:

$$\begin{aligned} E(\eta_i \zeta_k) &= 0 \quad \text{for all i, k} \\ E(\eta_i \eta_k) &= 0 = E(\zeta_i \zeta_k) \quad \text{for } i \neq k \\ E(\eta_i^2) &= E(\zeta_i^2) = b_i \end{aligned} \tag{25}$$

then the autocorrelation function of this process is:

$$R_x(\tau) = \sum_{i=1}^{\infty} b_i \cos \lambda_i \tau \tag{26}$$

In fact, Slutski[2] has shown that every stationary random process with an autocorrelation function as given in the form of equation (26) can be represented in the form of equation (24). Thus, there exists a gaussian random process with the same autocorrelation function as the autocorrelation function of the pseudo-noise process, as given in equation (22) and the power spectral densities of the two processes will also be equal.

The assumption is therefore made that the autocorrelation function and power spectral density of the pseudo-noise process is that of the gaussian random process as given in equation (24).

The autocorrelation function of the process $y(t)$, as given in equation (19), in which $x(t)$ is a gaussian random process and θ is uniformly distributed between 0 and 2π, has been found by Middleton[3] and is given by:

---

(2) Slutski, E. E., "Sur les fonctions aléatoires presque periodiques et sur la decomposition des fonctions aléatoires stationnaires en composantes." Actualités scientifiques et industrielles, no. 738, Hermann et Cie, Paris (1938), p. 33.

(3) Middleton, D. "The Distribution of Energy in Randomly Modulated Waves," Philosophical Magazine, Serial 7, Vol. 42, pp. 689-707, 1951.

$$R_y(\tau) = \frac{e^{-R_x(o)}}{2} e^{R_x(\tau)} \cos \omega_i \tau \tag{27}$$

Substituting, in the autocorrelation function from equation (22) the autocorrelation function of the randomly modulated carrier is then

$$R_y(\tau) = \frac{e^{-\sum_{i=1}^{\infty} b_i}}{2} \cos \omega_c \tau \prod_{i=1}^{\infty} e^{b_i \cos \lambda_i \tau} \tag{28}$$

Since the random process y(t) is wide sense stationary, the Wiener-Khintchine theorem can be used to obtain the power spectral density of y(t). The power spectral density $S_y(f)$ is then given by:

$$S_y(f) = 2\int_0^{\infty} \frac{e^{-\sum_{i=1}^{\infty} b_i}}{2} \cos \omega_i \tau \cos \omega \tau \prod_{i=1}^{\infty} e^{b_i \cos \lambda_i \tau} \, d\tau \tag{29}$$

$$= e^{-\sum_{i=1}^{\infty} b_i} \int_0^{\infty} \cos \omega_0 \tau \cos \omega \tau \prod_{i=1}^{\infty} \left[I_0(b_i) + 2 \sum_{n=1}^{\infty} I_n(b_i) \cos \lambda_i \tau \right] d\tau \tag{30}$$

where

$I_n(\xi)$ is a modified Bessel function of the first kind.

Performing the integration obtains

$$S_y(f) = e^{-\sum_{i=1}^{\infty} b_i} \left[\frac{\delta(f-f_c)}{2} + \frac{\delta(f+f_c)}{2}\right] * S_1(f) * S_2(f) * \cdots S_i(f) * \cdots \quad (31)$$

where

$$S_i(f) = I_o(b_i) + \sum_{n=1}^{\infty} I_n(b_i) \left[\delta(f+n\lambda_i) + \delta(f-n\lambda_i)\right] \quad (32)$$

NOTE

The symbol * denotes convolution.

3.1.3 Independent Uniform Phase Equivalent

As an alternate approach, the autocorrelation function of the pseudo-noise process can be considered as being that of a sum of cosine terms, each with a uniform phase distribution. Consider the random process given by:

$$x(t) = \sum_{i=1}^{\infty} \Delta\varphi_i \cos(\lambda_i t + \theta_i) \quad (33)$$

where the θ_i are mutually independent and uniformly distributed between 0 and 2π. Then the autocorrelation function of this process is:

$$R_x(\tau) = \sum_{i=1}^{\infty} \frac{\Delta\varphi_i^2}{2} \cos \lambda_i \tau \quad (34)$$

If the coefficient $\Delta\varphi_i^2/2$ is considered equal to the value of b_i, as given in equation (23), then the autocorrelation function and power spectral density of this process is given in equation (33) are the same as that of the pseudo-noise process.

Let the carrier be phase modulated by the process as given by equation (33), that is:

$$y(t) = \cos(\omega_i t + x(t) + \theta) \tag{35}$$

where θ is independent of the θ_i and is also uniformly distributed between 0 and 2π.

The autocorrelation function of the random process y(t) is then given by:

$$R_y(\tau) = E\left\{y(t)\,\overline{y(t+\tau)}\right\} \tag{36}$$

NOTE

The bar over the $y(t+\tau)$ denotes complex conjugate.
$E\{\ \}$ denotes expected value.

Substituting in equation (36) for y(t), obtains

$$R_y(\tau) = \frac{1}{4} e^{j\omega_c\tau} E\left\{ e^{j\sum_{i=1}^{\infty} \Delta\varphi_i \cos(\lambda_i (t+\tau) + \theta_i)}\, e^{j\sum_{i=1}^{\infty} \Delta\varphi_i \cos(\lambda_i t + \theta_i)} \right\}$$
$$+ \frac{1}{4} e^{-j\omega_c\tau} E\left\{ e^{-j\sum_{i=1}^{\infty} \Delta\varphi_i \cos(\lambda_i (t+\tau) + \theta_i)}\, e^{-j\sum_{i=1}^{\infty} \Delta\varphi_i \cos(\lambda_i t + \theta_i)} \right\} \tag{37}$$

Now, making use of the identity:

Now, making use of the identity:

$$e^{j\xi \cos\theta} = J_o(\xi) + \sum_{n=1}^{\infty} 2(j)^n J_n(\xi) \cos n\theta \tag{38}$$

Also, making use of the fact that the θ_i are independent, the autocorrelation function can then be written as:

$$R_y(\tau) = \frac{1}{4} e^{j\omega_c \tau} \prod_{i=1}^{\infty} E \left\{ \left[J_o(\Delta\varphi_i) + \sum_{n=1}^{\infty} 2(j)^n J_n(\Delta\varphi_i) \cos n(t+\tau) + \theta_i \right] \right.$$
$$\left. \left[J_o(+\Delta\varphi_i) + \sum_{n=1}^{\infty} 2(j)^n J_n(+\Delta\varphi_i) \cos n(\lambda_i t + \theta_i) \right] \right\} \tag{39}$$
$$+ \frac{1}{4} e^{-j\omega_c \tau} \prod_{i=1}^{\infty} E \left\{ \left[J_o(-\Delta\varphi_i) + \sum_{n=1}^{\infty} 2(j)^n J_n(-\Delta\varphi_i) \cos n(\lambda_1(t+\tau) + \theta_i) \right] \right.$$
$$\left. \left[J_o(-\Delta\varphi_i) + \sum_{n=1}^{\infty} 2(j)^n J_n(-\Delta\varphi_i) \cos n(\lambda_i t + \theta_i) \right] \right\}$$

Carrying out the expected value operation and making use of the identity

$$J_n(-x) = (-1)^n J_n(x) \tag{40}$$

the autocorrelation function is then given by:

$$R_y(\tau) = \frac{\cos \omega_c \tau}{2} \prod_{i=1}^{\infty} \left[J_o^2(\Delta\varphi_i) + 2 \sum_{n=1}^{\infty} J_n^2(\Delta\varphi_i) \cos n\lambda_i \tau \right] \tag{41}$$

The power spectral density of the modulated carrier is then found to be:

$$S_y(f) = \left[\frac{\delta(f - f_c)}{4} + \frac{\delta(f + f_c)}{4}\right] * S_1(f) * S_2(f) * \ldots \tag{42}$$

where $S_i(f)$ is the power spectral density given by

$$S_i(f) = J_o^2(\Delta\varphi_i) + \sum_{n=1}^{\infty} J_n^2(\Delta\varphi_i)\ \delta(f - n\lambda_i) + \delta(f + n\lambda_i)$$

$$= \sum_{n_i=-\infty}^{\infty} J_{n_i}^2(\Delta\varphi_i)\ \delta(f + n\lambda_i) \tag{43}$$

Thus far, the pseudo-noise sequence has been considered to be the ideal (unfiltered) sequence. If the output of the pseudo-noise shift register is filtered, then the power spectral density of the modulation will be given by

$$S_m(f) = \left|\frac{H(j\omega)}{j\omega}\right|^2 S_x(f) \tag{44}$$

where

$H(j\omega)$ = transfer function of filter
$S_x(f)$ = pseudo-noise power spectral density

If frequency modulation were used rather than phase modulation, then the modulation power spectral density would be given by:

$$S_m(f) = \left|\frac{H(j\omega)}{j\omega}\right|^2 S_x(f) \tag{45}$$

The above procedure gives the power spectral density of the carrier when angle modulated by a pseudo-noise sequence either filtered or unfiltered. Although the expression obtained is rather formidable, being the convolution of an infinite

number of terms, each term being an infinite series, it should be possible to reduce the complexity. Since the modulation index ($\Delta\varphi_i$) will be small, it should be possible to neglect higher-order Bessel functions. Also, it is possible to consider only the harmonic components of the pseudo-noise spectrum out to the second null, as shown in Figure 3-1. Thus, the number of terms to be convolved would be 2p terms, which is still a rather large number. Even with these simplifications, a computer would be necessary to obtain an answer.

3.2 REACQUISITION ANALYSIS

A preliminary investigation of methods for reducing the reacquisition time for PN sequences has been conducted. Use of a conventional intercept receiver* has been emphasized, with the goal of obtaining reacquisition within 0.5 second after a two-second signal dropout. The results of this investigation are reported in this sub-section.

3.2.1 Frequency and Time Uncertainty

At maximum range (4000 nautical miles), the determining factor in frequency uncertainty after a dropout is the ability of the spacecraft equipment to "remember" the doppler frequency existing at the time that the signal was lost.** If it is assumed that a doppler memory is available, and that it is accurate to 1 percent of the maximum doppler offset, the frequency uncertainty at 2 KMHz is approximately 500 Hz.

To determine the time uncertainty at 4000 nautical miles, it is necessary to calculate the change in spacecraft position during the two-second signal dropout. As the range rate (for a circular orbit) is approximately two nautical miles/second, a change of about 50 microseconds in the delay (two-way) results.

---

* In these receivers, a VCO is linearly swept over the frequency uncertainty band until the presence of a signal is sensed in a narrow band threshold detector. At this point, the sweep is stopped and the tracking filter assumes control of the VCO for final pull-in.

** If no doppler memory is available, it may be necessary to employ doppler wipeout and the procedure used for initial acquisition.

However, the doppler memory can be used to reduce this uncertainty to 0.5 microseconds by controling the shifting rate of the PN generator.

At minimum range the uncertainty situation is substantially different. Since $\dot{r} \approx 0$, only a small doppler and time uncertainty exist. However, the large range acceleration values encountered can, in the worst case, necessitate a "chase" of the rapidly changing doppler frequency. Assuming r = 90 nautical miles, a doppler rate of approximately 5 KHz/seconds exists (at 2KMHz). If no doppler rate memory is provided*, the total doppler uncertainty after a two-second dropout is 10 KHz, and the frequency could still be moving away from the expected value at about 5 KHz/second (worst case).

3.2.2 Filter Analysis

A "worst-case" analysis of the preceding requirements indicated that the 1/2 second reacquisition goal could not be met with satisfactory confidence when using any given narrow band filter for all the signal conditions encountered in the system. The principal reason for this is the need for a narrow band filter to provide a satisfactory SNR at the maximum range, and the need for a wider band filter to "chase" the rapidly varying doppler at the minimum range. Therefore, several two-filter combinations were evaluated to determine their suitability for operation over the entire AROD operating envelope. A compromise solution evolved with the following characteristics:

a. A doppler memory accurate to 1 percent.

b. A swept filter 70 Hz wide for use at altitudes between 400 and 2000 nautical miles.

c. A swept filter 200 Hz wide for use at altitudes between 90 and 400 nautical miles.

An evaluation of this system at the critical points in the operating envelope follows. It is assumed that the available signal power-to-noise power density ratio at 4000 nautical miles is 2000 Hz; this allows a 10 db margin (with respect

---

* The presence of a doppler rate memory would effect a major reduction in this problem.

to the parameters assumed in the Fifth Quarterly Report) for filter off-centering, slight code mismatches, and transmission or reception perturbations. Further, it is assumed that the PN bit rate is approximately 1 Mbps (for either a pure PN or hybrid system).

At r = 4000 nautical miles, the use of a "dwell time" of 1/70 second yields a signal energy-to-noise power density ratio $\left(\frac{E}{N_o}\right)$ of approximately 30; this will result in a probability of detection[4] of approximately 99.5 percent and a false alarm probability of 10^{-6}, which should provide satisfactory performance. The 500 Hz uncertainty band can be swept in

$$t_s = \frac{500}{(70)(70)} \approx 0.1 \text{ second}$$

since the 0.5 microsecond time uncertainty is less than one PN bit. After the swept filter has located the carrier to within 70 Hz, the phase-lock loop must pull in. This pull-in time is given by:*

$$t_{pi} = \frac{\Omega^2}{2\zeta \omega_n^3} = \frac{[2\pi(70)]^2}{2(.707)(80)^3} \approx 0.2 \text{ second}$$

Thus, the carrier loop is locked in well within the 0.5 second goal.

When r = 2000 nautical miles (directly overhead for a 2000 nautical miles circular orbit), the doppler rate is approximately 100 Hz/second. For the "worst case chase," with a 70 Hz filter, the chase time (t_c) can be obtained from

$$(70)^2 t_c = 2(100) + 100 t_c$$

which yields $t_c \approx 0.04$ second

---

(4) Skolnik, M. I., "Introduction to Radar Systems," p. 437, McGraw-Hill, 1962.

* Fifth Quarterly Report, p. 1-24. (The loop parameters used are those suggested on p. 1-28.)

The frequency uncertainty (Ω) due to the doppler rate is 2(100) = 200 Hz, which yields a pull-in time for the carrier phase-lock loop of approximately 0.05 second.* The total time is, again, well within the goal, and the probability of detection will be increased because of the larger SNR.

The evaluation of the system for a 90 nautical mile circular orbit follows. At the maximum range (600 nautical mile), the 1000 Hz uncertainty band can be swept by the 200 Hz filter in:

$$t_s = \frac{1000}{(200)^2} = 0.025 \text{ second},$$

and the phase-lock loop pull-in time is approximately 0.04 second. Even if the larger $\dot{r}$ necessitates a search through two PN bits, the reacquisition time is well below the goal. At the minimum range (90 nautical miles), the worst-case chase time is found from:

$$(200)^2 t_c = 10{,}000 + 5000\ t$$

to be $t_c \approx 0.3$ second, and the loop pull-in time is less than 0.001 second.

For the 400 nautical miles switching altitude, both filters must be evaluated. Table 3-1 presents the results of the calculations for reacquisition time for the carrier loop for this altitude.

3.2.3 Conclusions

It has been shown that reacquisition of a PN-modulated carrier can be achieved in less than 1/2 second with the conventional intercept receiver. A doppler memory accurate to 1 percent, and a switchable swept filter are required. The presence of more elaborate equipment (for example, a doppler rate memory, variable detection thresholds, or sequential detectors) could reduce the reacquisition time still further.

---

* Linear amplification in the spacecraft receiver has been assumed, and, therefore, the factor ($\zeta \omega_n^3$) is proportional to R^2.

Table 3-1

REACQUISITION TIME CALCULATIONS FOR
h = 400 NAUTICAL MILES

Filter	5° Elevation		90° Elevation	
	t_s (sec)	t_{pi} (sec)	t_c (sec)	t_{pi} (sec)
70 Hz	0.18	0.025	0.45	0.01
200 Hz	0.02	0.2	0.05	0.08

It is recommended that further investigations of optimal reacquisition techniques be conducted. Such matters as sequential detection, autocorrelation properties of PN sequences integrated for less than their full period (and when the frequency is different from the expected value), and optimal allocation of reacquisition time between t_s and t_{pi} should be analyzed further. It is quite possible that an optimal reacquisition system could permit initial acquisition with the PN modulation still on the (doppler wiped-out) carrier, thereby substantially improving the interference rejection properties of AROD during acquisition.

Appendix A

SEMICONDUCTOR DEVICES

The implementation of the Memory-Aided Phase-Locked Loop described in Section 2 is largely dependent upon the characteristics, and circuit capabilities afforded by two recently-available, advanced semiconductor devices. These are differential operational amplifiers in monolithic integrated form and metal oxide semiconductor field effect transistor (MOSFET) devices.

The particular integrated operational amplifier found to be most satisfactory for AROD purposes is the Fairchild μA-702) device in eight-lead TO-5 cans. The manufacturer's specification and data sheet is herein reproduced for reference. The μA-702 is a high-performance DC amplifier constructed on a single silicon chip, using planar-epitaxial integrated circuit techniques. It is a high-gain operational type amplifier meant for use with external feedback elements to determine operating characteristics. Significant features are low DC offset and drift, wide bandwidth, low power consumption, and large output swing.

The MOSFETs employed are the General Micro-Electronics (GME) 2N3609, a dual matched pair, and the Fairchild FI-100 units, the respective specification and data sheets of which are included for reference. The outstanding properties of the MOSFETs pertinent to this application (Section 2) are their extremely high input impedances ($> 10^{12}$ ohms) and their zero offset switching capabilities in contrast to conventional bipolar (injection) transistors. These unique properties are important for implementation of long-time analog signal storage with reasonable sized capacitors and analog signal switching functions, respectively.

μA-702 HIGH GAIN, WIDEBAND DC AMPLIFIER

FAIRCHILD LINEAR INTEGRATED CIRCUITS

GENERAL DESCRIPTION - The μA-702 is a complete d-c amplifier constructed on a single silicon chip, using the Fairchild Planar epitaxial process. It is intended for use as an operational amplifier in miniaturized analog computers, as a precision instrumentation amplifier, or in other applications requiring a feedback amplifier useful from d-c to 10 mc. Fairchild Application Note APP-105 describes the amplifier and some of its uses.

ABSOLUTE MAXIMUM RATINGS

Total Supply Voltage Between V^+ and V^- Terminals	21.0 Volts
Peak Load Current	10 mA
Maximum Internal Power Dissipation	250 mW
Storage Temperature Range	-65°C to +150°C
Operating Temperature Range	-55°C to +125°C

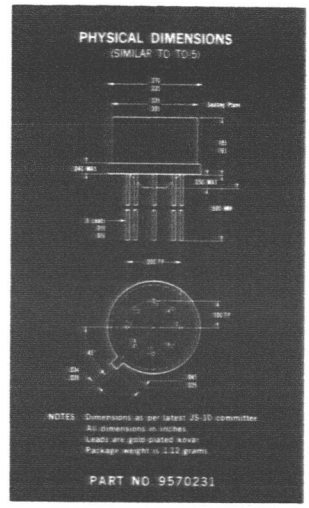

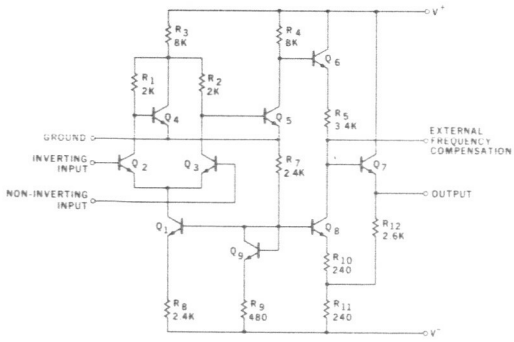

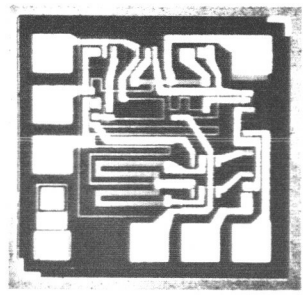

μA-702 DIE
45 x 45 mils

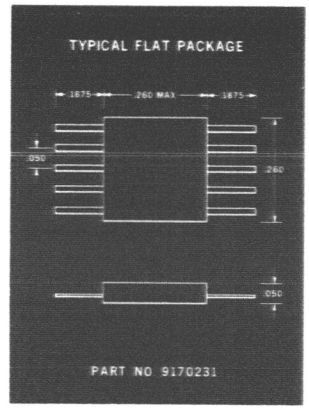

TO-5 CONNECTION DIAGRAM (TOP VIEW)

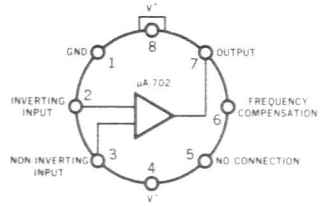

FLAT PACKAGE CONNECTION DIAGRAM (TOP VIEW)

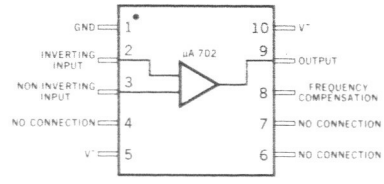

ELECTRICAL CHARACTERISTICS (25°C Free Air Temperature unless otherwise noted)

PARAMETER	CONDITIONS	$V^+ = 12V$ $V^- = -6V$ Min	Typ	Max	$V^+ = 6V$ $V^- = -3V$ Min	Typ	Max	Units
Input Offset Voltage (ΔV_{in})	$R_S \leq 2K$	-	2	5	-	2	5	mV
Input Offset Current (ΔI_{in})		-	.7	2	-	.5	2	μA
Input Impedance (R_{in})		8	25	-	12	40	-	KΩ
Input Bias Current (I_{in})		-	4	10	-	2.5	7	μA
Input Common Mode Range		-4.0	-	+.5	-2.0	-	+.5	V
Common Mode Rejection Ratio (CM_{RR})	$f \leq 1Kc$	70	80	-	70	80	-	db
Open Loop Voltage Gain (A_{vo})		1400	2600	4000	380	700	1000	
Open Loop Bandwidth (B_o)		.7	1.1	-	.7	1.2	-	mc
Output Impedance (R_o)		-	200	500	-	300	700	Ω
Output Voltage Swing	$R_L \geq 100$ K	±5.0	±5.3	-	±2.5	±2.7	-	V
Average Temperature Coefficient of Input Offset Voltage	$25°C \leq T_A \leq 125°C$	-	5	-	-	5	-	μV/°C
	$-55°C \leq T_A \leq 25°C$	-	10	-	-	10	-	μV/°C
Input Offset Voltage	$R_S \leq 2K$, $-55°C \leq T_A \leq +125°C$	-	-	6	-	-	6	mV
Input Offset Current	$-55°C \leq T_A \leq 125°C$	-	-	3	-	-	3	μA
Open Loop Voltage Gain	$-55°C \leq T_A \leq 125°C$	1000	-	-	-	-	-	
Input Bias Current	$T_A = -55°C$	-	-	20	-	-	14	μA
DC Supply Power		-	70	110	-	17	27	mW
Positive Supply Voltage Sensitivity		-	50	-	-	100	-	μV/V
Negative Supply Voltage Sensitivity		-	100	-	-	200	-	μV/V

TYPICAL PERFORMANCE CURVES OF μA-702 AMPLIFIER

ALL GRAPHS WITH $V^+ = 12V$, $V^- = -6V$, $T_A = +25°C$, UNLESS SPECIFIED

VOLTAGE TRANSFER CHARACTERISTIC

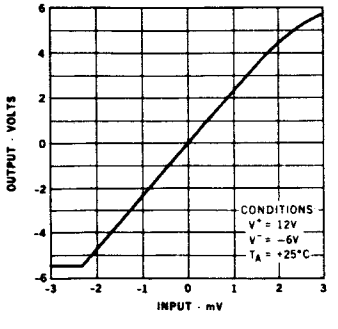

OPEN LOOP VOLTAGE GAIN AS A FUNCTION OF TEMPERATURE

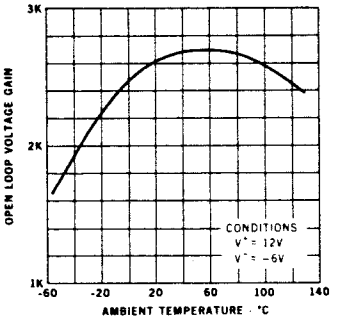

FI 100

P-CHANNEL MOS FIELD-EFFECT TRANSISTOR

DIFFUSED SILICON PLANAR II DEVICE

The FI100 is a silicon PLANAR II (Note 1) MOS Field-Effect Transistor designed for enhancement mode operation. As a chopper or multiplex switch, the device features zero offset voltage, large signal switching capability, and a high OFF to ON impedance ratio. The MOS unit can be easily direct-coupled to form all basic logic configurations having much higher fan-outs than conventional bi-polar transistors. In amplifier application, the enhancement mode operation permits extremely high input impedance ($>10^{13}$ Ohms), DC coupling between stages and excellent DC to high frequency amplifier performance.

PHYSICAL DIMENSIONS

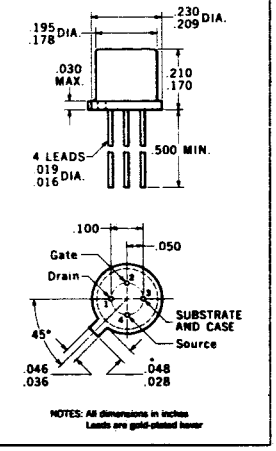

ABSOLUTE MAXIMUM RATINGS (Note 2)

Maximum Temperatures		
	Storage Temperature	-65°C to +200°C
	Operating Junction Temperature	-65°C to +175°C
Maximum Power Dissipation		
	Total Dissipation at 25°C Case Temperature	1.0 Watt
	at 25°C Ambient Temperature	0.35 Watt
Maximum Voltage & Current		
V_{DSS}	Drain to Source Voltage	-30 Volts
V_{GSS}	Gate to Source Voltage (Note 3)	±40 Volts
V_{GSS}	Gate to Source Voltage Transient (Note 3)	±60 Volts
I_D	Drain Current	-35 mA

HANDLING INSTRUCTIONS

This is an insulated gate device wherein the insulation is a very thin layer of glass (Si 0_2) between the control (gate) electrode and the area beneath. Due to low capacity (C_{gs}) and high leakage resistance (R_{GS}) of the gate, slight electrostatic charges can result in large voltages capable of damaging the dielectric.

Storage	All four leads should be in contact with each other
Testing	Grasp the test chassis prior to insertion of the device into any circuit or test equipment. Additional precautions should be taken to ground all soldering iron tips, etc.

ELECTRICAL CHARACTERISTICS (25°C Free Air Temperature, Substrate Connected to Source)

Symbol	Characteristic	Min.	Typ.	Max.	Units	Test Conditions
I_{DSS}	Drain Leakage Current		0.05	0.5	nA	V_{GS} = 0 V_{DS} = 15 V
BV_{DSS}	Drain Breakdown Voltage	-30	-50		Volts	V_{GS} = 0 I_D = 10 μA
V_{GST}	Gate Threshold Voltage	-2.5	-4.5	-6.0	Volts	V_{GD} = 0 I_D = 10 μA
I_{SDS}	On Current	-3.0	-6.0	-12	mA	V_{GS} = V_{DS} = -15 V
R_{GS}	Gate Leakage Resistance	10^{13}	10^{15}		Ohms	V_{GS} = V_{GD} = -15 V
r_d	Dynamic Drain Resistance, f = 1 Kc		150		Kohms	V_{GS} = V_{DS} = -10 V
C_{gs}	Gate to Source (plus gate to channel) Capacitance, f = 1 mc		2.5	3.5	pf	V_{GS} = V_{DS} = -10 V
C_{gd}	Gate to Drain Capacitance, f = 1 mc		0.4	1.0	pf	V_{GS} = V_{DS} = -10 V
C_{ds}	Output Capacitance		1.9	3.0	pf	V_{GS} = V_{DS} = -10 V
Y_{fs}*	Gate to Drain Transconductance	300	600		μmhos	V_{GS} = V_{DS} = -10 V

(See notes on back page) *Also Known as G_m

THIS DATA SHEET IDENTIFIES A PARTICULAR LABORATORY DESIGN OF SEMICONDUCTOR PRODUCT. THE TYPE NUMBER AND PRELIMINARY SPECIFICATIONS ARE SUBJECT TO CHANGE. NO OBLIGATIONS ARE ASSUMED FOR NOTICE OF CHANGE OR FUTURE MANUFACTURE OF THE PRODUCT UNLESS OTHERWISE ARRANGED

FAIRCHILD SEMICONDUCTOR
A DIVISION OF FAIRCHILD CAMERA AND INSTRUMENT CORPORATION

MANUFACTURED UNDER ONE OR MORE OF THE FOLLOWING U. S. PATENTS: 2981877, 3025589, 3064167, 3108359, 3117260. OTHER PATENTS PENDING.

TYPICAL ELECTRICAL CHARACTERISTICS

DRAIN CHARACTERISTICS

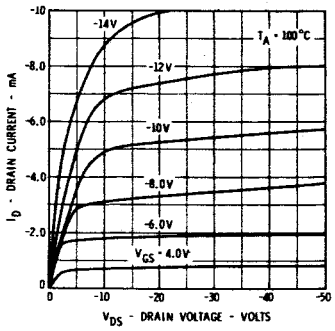

DRAIN CHARACTERISTICS

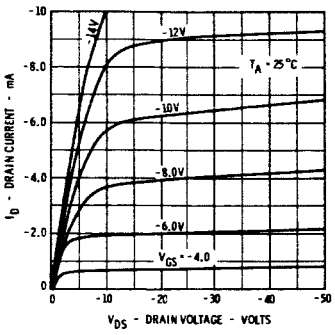

DRAIN CHARACTERISTICS

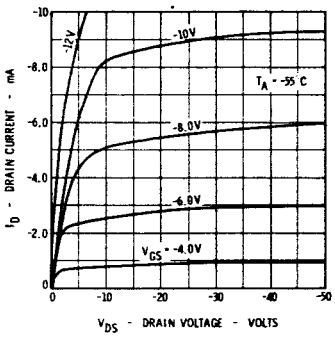

+100°C

+ 25°C

-55°C

DRAIN CHARACTERISTICS

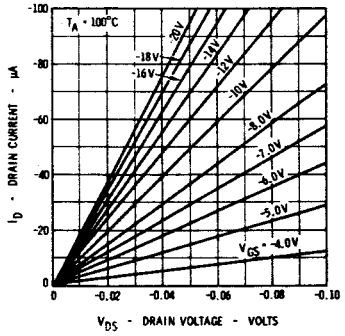

DRAIN CHARACTERISTICS

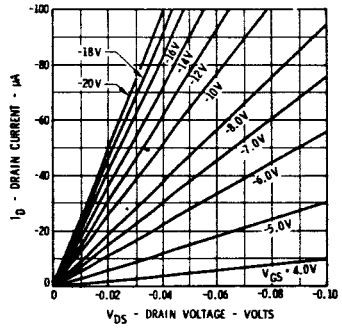

DRAIN CHARACTERISTICS

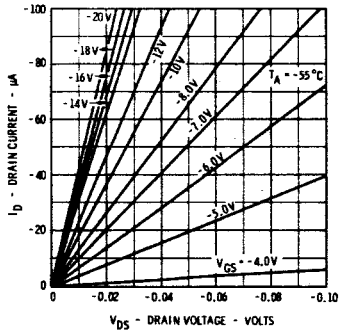

ELECTRICAL SYMBOL

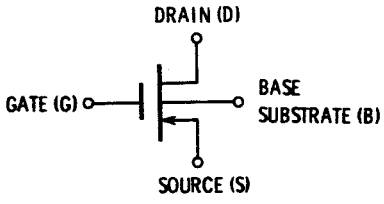

SMALL SIGNAL CIRCUIT MODEL

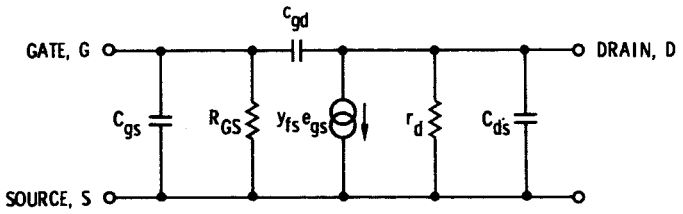

NOTES:

(1) PLANAR II is the process which prevents ion migration in planar oxides under the influence of heavy (e.g., 2×10^6 volts/cm) electric fields.

(2) These ratings are limiting values above which the serviceability of any individual semiconductor device may be impaired.

(3) Electrostatic potentials which may be generated by improper storage, handling, or testing, could destroy the dielectric if they exceed this rating. The insertion of leads into polystyrene can produce potentials of 300 volts or more.

313 FAIRCHILD DRIVE, MOUNTAIN VIEW, CALIFORNIA, (415) 962-5011, TWX: 910-379-6435

In Micro-electronics it's GME

1005 INTEGRATED DUAL P-CHANNEL METAL OXIDE SILICON FIELD EFFECT TRANSISTORS

TECHNICAL DATA SHEET

AUGUST 1964

Tentative Specifications

This five-terminal device contains two P-channel MOS Field-Effect Transistors designed for enhancement mode operation, diffused into one monolithic chip. As a result of the monolithic structure, this device has excellent thermal tracking between the two triodes. The device is well suited for a wide variety of applications, such as high input impedance differential amplifiers, modulators, demodulators and choppers to mention only a few.

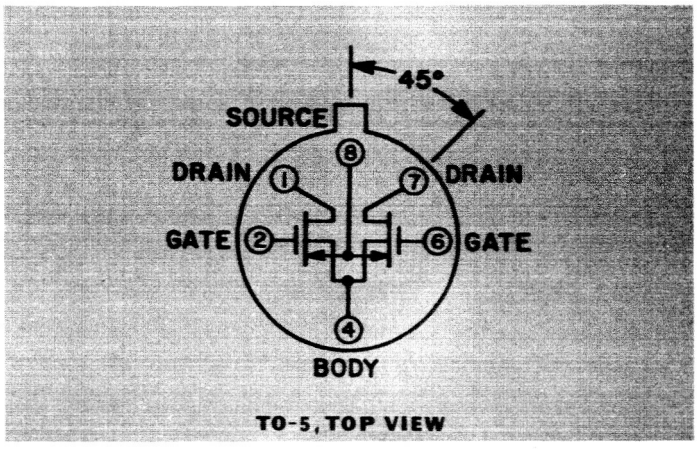

TO-5, TOP VIEW

Typical Applications of the Dual 1005 MOS FET Device

(All body leads tied to source leads unless otherwise noted)

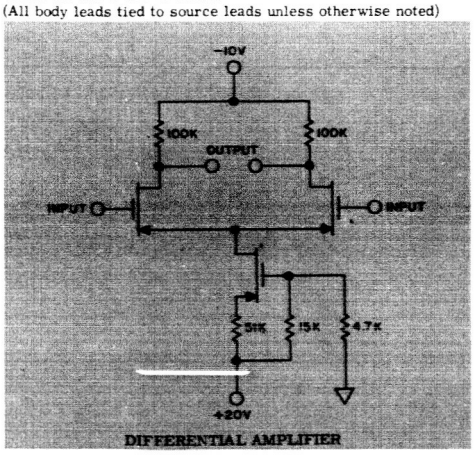

DIFFERENTIAL AMPLIFIER

Absolute Maximum Ratings
(Steady State Except When Otherwise Stated)

Maximum Junction Temperature	-55°C to +125°C
Dissipation (Total Device)	
at Case Temperature of 25°C	1.0 watt
at Case Temperature of 100°C	.2 watt
at Ambient Temperature of 25°C	.35 watt
Maximum Voltages (Body Lead Tied to Source Lead)	
V_{DSS} Drain to Source Voltage	-25 volts
V_{GSS} Gate to Source Voltage	-25 volts
V_{GSS} Gate to Source Voltage Transient	±60 volts

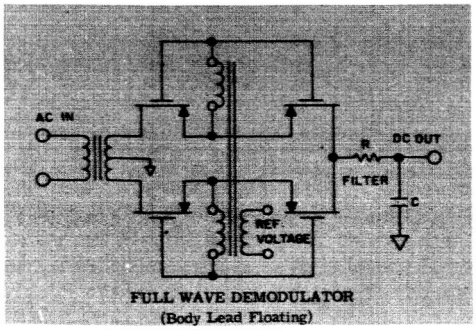

FULL WAVE DEMODULATOR
(Body Lead Floating)

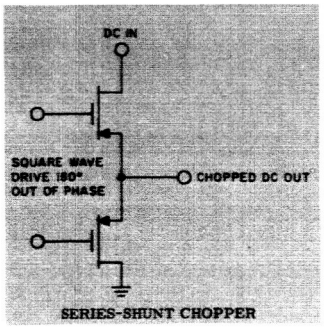

SERIES-SHUNT CHOPPER

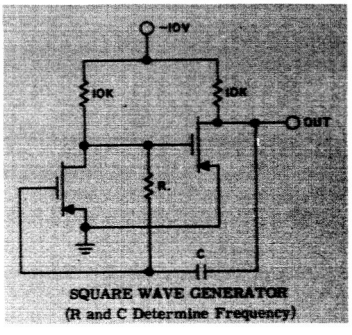

SQUARE WAVE GENERATOR
(R and C Determine Frequency)

General Micro-electronics Inc.

2920 SAN YSIDRO WAY • SANTA CLARA, CALIFORNIA 95051 • TWX: (408) 737-9961 • PHONE (408) 245-2966

2430 Pennsylvania Ave., N.W. Suite 115, Washington, D.C. (202) 338-7077

9911 Inglewood Blvd. Suite 102, Inglewood, Calif. (213) 677-6111

1250 W. Dorothy Ln. Dayton, Ohio (513) 298-0249

Benson Manor, Suite 114 B, Washington Ln., Jenkintown, Penn. (215) 885-0430

1643 Beacon St. Waban, Mass. (617) 332-5880

Typical Characteristic Curves

DRAIN CHARACTERISTICS AT 125°C

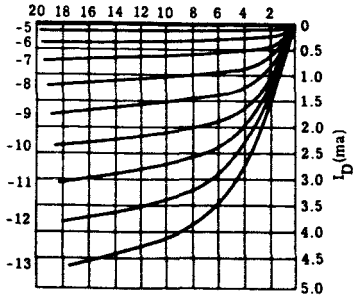

DRAIN CHARACTERISTICS AT 25°C

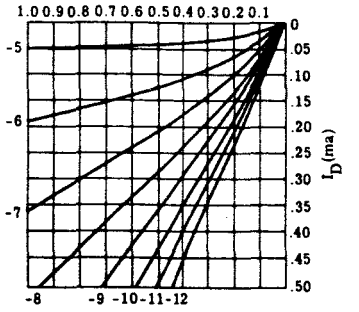

DRAIN CHARACTERISTICS AT -200°C

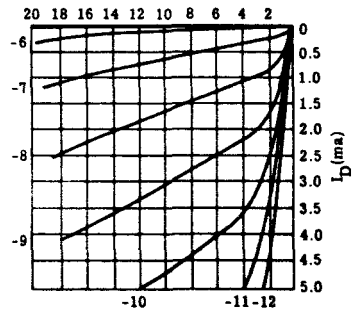

DRAIN CHARACTERISTICS AT 25°C

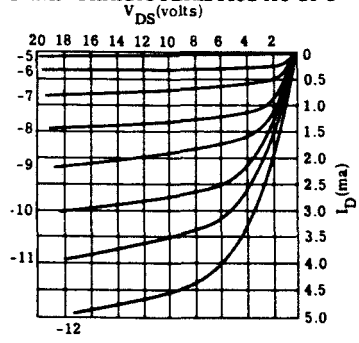

TURN-ON CHARACTERISTICS AT 25°C

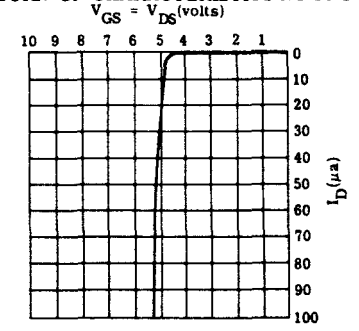

TURN-ON CHARACTERISTICS AT 25°C

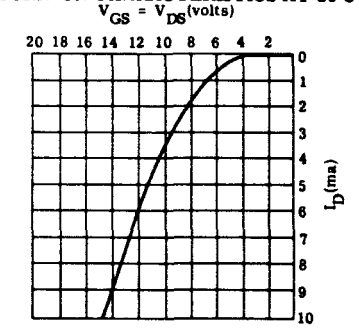

Electrical Characteristics at 25°C (Each Triode)

(Unless otherwise specified source lead connected to body lead for all values.)

Note 1: Drain and gate shorted to body.

Symbol	Characteristic	Value Min.	Typ.	Max.	Units	Test Conditions
V_{GST}	Gate Threshold Voltage	-4	-5	-6	volts	$V_{DS} = V_{GS}$, I_D = 10 μa
g_{FS}	DC Transconductance	400	650	—	μmhos	$V_{DS} = V_{GS}$, I_D = 10 ma
g_{fs}	AC Transconductance	400	650	—	μmhos	$V_{DS} = V_{GS}$, I_D = 1 ma
g_{fs}	AC Transconductance	150	200	—	μmhos	$V_{DS} = V_{GS}$, I_D = 100 μa
I_{DSS}	Drain Leakage Current	—	5	35	na	V_{GS} = 0, V_{DS} = -20 volts
I_{SDS}	Source Leakage Current (Note 1)	—	5	35	na	V_{GD} = 0, V_{SD} = -20 volts
BV_{DSS}	Drain-Source Breakdown Voltage	-30	-50	—	volts	V_{GS} = 0, I_D = 10 μa
BV_{SDS}	Source-Drain Breakdown Voltage (Note 1)	-30	-50	—	volts	V_{GS} = 0, I_S = 10 μa
R_{IS}	Gate Leakage Resistance	10^{13}	$>10^{14}$	—	ohms	V_{DS} = 0, V_{GS} = -20 volts
r_d	Dynamic Drain Resistance	25	50	—	kohms	$V_{DS} = V_{GS}$, I_D = 1 ma
r_d	Dynamic Drain Resistance	250	400	—	kohms	$V_{DS} = V_{GS}$, I_D = 100 μa
r_d	Dynamic Drain Resistance	—	1000	1300	ohms	V_{GS} = -10 volts, V_{DS} = 0
r_d	Dynamic Drain Resistance	—	450	550	ohms	V_{GS} = -20 volts, V_{DS} = 0
C_{gs}	Gate-Source Capacitance	—	3.5	4.0	pf	$V_{DS} = V_{GS}$, I_D = 1 ma
C_{gd}	Gate-Drain Capacitance	—	1.5	2.0	pf	$V_{DS} = V_{GS}$, I_D = 1 ma
C_{ds}	Drain-Source Capacitance	—	1.5	2.0	pf	$V_{DS} = V_{GS}$, I_D = 1 ma

Matching Characteristics at 25°C (Unless Otherwise Noted)

Symbol	Characteristic	Value Min.	Typ.	Max.	Units	Test Conditions
g_{fs_1}/g_{fs_2}	AC Transconductance Ratio (Note 2)	0.8	-	1.0	-	$V_{DS} = V_{GS}$, I_D = 100 μa
$\lvert V_{GST_1} - V_{GST_2} \rvert$	Gate Threshold Voltage Differential	-	-	100	m volts	V_{DS} = -10 volts, I_D = 100 μa
$\lvert \Delta(V_{GST_1} - V_{GST_2}) \rvert$	Gate Threshold Voltage Differential Change (T_A = -55°C to +125°C)	-	20	-	m volts	V_{DS} = -10 volts, I_D = 100 μa

(Source Lead Connected to Body Lead for All Values)

Note 2: Lowest of the two g_{fs} readings is taken as g_{fs_1} for the purposes of this ratio.